Microplasma : a new generation of technology for functional nanomaterial synthesis

Document Version:
Accepted manuscript including changes made at the peer-review stage

Please check the document version of this publication:

• A submitted manuscript is the version of the article upon submission and before peer-review. There can be important differences between the submitted version and the official published version of record. People interested in the research are advised to contact the author for the final version of the publication, or visit the DOI to the publisher's website.
• The final author version and the galley proof are versions of the publication after peer review.
• The final published version features the final layout of the paper including the volume, issue and page numbers.

Link to publication

CrossMark

2 REVIEW ARTICLE

3 Microplasma: A New Generation of Technology
4 for Functional Nanomaterial Synthesis

5 **Liangliang Lin[1] · Qi Wang[1]**

8 **Abstract** Plasma technology has been widely applied in the ozone production, material
9 modification, gas/water cleaning, etc. Various nanomaterials were produced by thermal
10 plasma technology. However, the high temperature process and low uniformity products
11 limit their application for the high value added chemicals synthesis, for example the
12 functional materials or the temperature sensitive materials. Microplasma has attracted
13 significant attentions from various fields owing to its unique characteristics, like the high-
14 pressure operation, non-equilibrium chemistry, continuous-flow, microscale geometry and
15 self-organization phenomenon. Its application on the functional nanomaterial synthesis
16 was elaborately discussed in this review paper. Firstly, the main physical parameters were
17 reviewed, which include the electron temperature, electron energy distribution function,
18 electron density and the gas temperature. Then four representative microplasma configu-
19 rations were categorized, and the proper selection of configuration was summarized in light
20 of different conditions. Finally the synthesis, mechanism and application of some typical
21 nanomaterials were introduced.

A1 ✉ Qi Wang
A2 Q.Wang1@tue.nl

A3 [1] Micro Flow Chemistry and Process Technology, Department of Chemical Engineering and
A4 Chemistry, Eindhoven University of Technology, Den Dolech 2, 5600 MB Eindhoven,
The Netherlands

Ⓐ Springer

Introduction

Plasma is generally referred to as the fourth state of substrate, which is usually described as a mixture of fully or partially ionized gas [1]. Due to the presence of a diversity of energetic species such as electrons, ions, atoms, charged particles and excited molecules, plasma is applied to stimulate the chemistry especially the ones that can hardly be realized in mild ways, e.g. methane reforming [2–5], CO_2 conversion [6–8], VOC decomposition [9–11], surface treatment of polymer surfaces [12–15], medical treatment [16–20], material synthesis [21–25], etc. Plasma technology is commercialized and industrialized in the fields of ozone production, material surface modification, air/water cleaning, medical facilities, etc., which has already shown promising energy effects and economic benefits.

Nanomaterial synthesis is widely realized through non-plasma related methods, like chemical vapor deposition (CVD) [26–28], solvothermal routes [29–31], sol–gel methods [32–34], laser ablation [35–37], etc. Fine quality products could be obtained when the starting materials and processes were properly chosen and controlled by non-plasma methods. However, it's normally difficult to control the distribution of nanoparticle size due to the extremely long reaction time. Besides, the post treatments like washing or annealing to improve products' chemical purity or crystallinity are always required, resulting in complex steps which are time and energy consuming, thus limiting their industrial applications [38].

Compared with the named non-plasma technology which uses thermal energy from high temperature, a plasma-based technology uses energy from plasma discharges to activate precursors. Therefore, it allows the use of temperature sensitive or low reactive precursors. Besides, the plasma-based technology always has unique properties such as the ability to produce nanomaterials with the freedom of choice in constituents, along with "chosen" properties such as the crystallinity and morphology [39]. Series of plasma-based technology like spark plasma sintering, thermal plasma expansion or plasma-enhanced chemical vapor deposition (PECVD) were developed over decades. And a wide range of nanomaterials were synthesized under different conditions, for example, carbides nano-sized powders such as WC [40], TiC [41], TiCN [42], SiC [43–45], nitrides nanomaterials such as TiN [46–49], AlN [50–52], Mg_3N_2 [53], GaN [54], BN [55], oxides nanomaterials such as Al_2O_3 [56], [57], SnO_2 [58], V_2O_5 [59], ZnO [60], TiO_2 [61] and metal nanoparticles such as Ag, Cu, Fe [62–64].

Plasma was also applied for producing carbon materials over the past decades, among which two typical examples were carbon nanotubes (CNT) [65–69] and carbon black (CB) [70–72]. Nowadays one intensively studied field is the production of carbon black by thermal plasma, where there were two competing and patented processes exist [73]. One was the Kvaerner process developed in Norway, in which carbon black and hydrogen gas were produced from the hydrocarbons like methane, biogas or natural gas by thermal plasma [74, 75]. Another was the three-phase arc plasma process developed in France [71, 76–78], in which hydrocarbons were decomposed in an arc plasma reactor. Compared with other method, both methods are very energy efficient and can almost convert all the hydrocarbons.

Till now, a number of plasma processes for nanomaterial fabrication were developed. Currently there has been an increase in the number of reports about the plasma assisted nanomaterial synthesis. However, most of the existed plasma technology for nanomaterial synthesis are normally designed and operated at low pressure which necessitates expensive vacuum equipment and is not in favor of industrialization. The spatial scale of the

72 reaction volume involved in these reactors is always large, leading to the difficulty to
73 control a uniform temperature, concentration and residence time distribution environment
74 for particle nucleation and growth, thus the produced products are commonly characterized
75 by partial agglomeration and wide size distribution [79]. In addition, the surmised
76 mechanism for nanomaterial synthesis includes the collisions between radical moieties in
77 gas phase, which can be enhanced substantially at high pressures [80]. Therefore, a plasma
78 technology for high quality nanomaterial synthesis which can be easily operated and
79 controlled under atmospheric pressure is needed.

80 This could possibly be addressed by the recent developed technique of microscale
81 plasma - microplasma, which is a special category of plasma confined within sub-mil-
82 limeter length scale in at least one dimension [81]. In virtue of the increased surface-to-
83 volume ratio and the decreased electrode spacing, microplasma boasts several key
84 advantages compared with conventional plasma: the high-pressure operation, non-equi-
85 librium chemistry, continuous-flow, microscale geometry and self-organization phe-
86 nomenon [80]. In general, it possesses the characteristics of the conventional plasma but
87 combined with microscale geometry, resulting in a new and novel branch of plasma
88 science. Based on these reasons, microplasma is intensively researched in recent years for
89 their potential applications in a wide range of fields.

90 Besides the above mentioned unique chemistry, microplasma offers the possibility of
91 preserving strong non-equilibrium state in a wide range of gas mixtures [82], allowing for
92 high reaction rates, and enabling a large number of fast and efficient high-throughput
93 processes [79]. Since the micro reactor geometry can limit the particle nucleation and
94 growth by controlling a short residence time with a narrow RTD, the production of narrow-
95 size distributed nanoparticles is easy to achieve. On the other hand, the microscale also
96 makes it easy to realize discharge under high pressure, along with the reduction of safety
97 risks when handling toxic materials. By virtue of the above mentioned advantages, in latest
98 years there have been more researches on functional nanomaterial synthesis by micro-
99 plasma, although it retains a disadvantage of low product output as a result of the small
100 scale dimension. In this paper, the state of the art for the fabrication of nanomaterials by
101 microplasma is going to be discussed.

102 The comparison of different methods for nanomaterial synthesis was summarized in
103 Table 1.

Table 1 Methods for nanofabrication with their advantages and drawbacks

Methods	Advantages	Drawbacks
Non-plasma related methods	Products with high purity and good quality when raw materials and processes are well selected and controlled	High energy consumption Long reaction time Difficult to control the process
Conventional plasmas	Simple, clean, efficient and flexible Products with chosen constituents	Requires low pressure or high temperature Expensive reactors Products with wide size distribution
Micro-plasmas	Atmospheric pressure operation Simple, efficient, safe, economical Products with high uniformity	Low product output, but can be solved by microplasma arrays

104 **Microplasma Parameters and Applications**

105 According to the Paschen's law, the breakdown voltage of a discharge for a certain gas is a
106 function of the pressure and the gap length between two electrodes. Microplasma is a type of
107 plasma which is generated in a micro scale discharge gap (at submillimeter level) under
108 atmospheric pressure. Except the advantages of short residence time and narrow RTD,
109 another significant feature of microplasma is its non-equilibrium state, in which the gas
110 temperature T_g is much lower than the electron temperature T_e. There are mainly two reasons.
111 Firstly, the electrons exchange energy via collisions with the other radicals such as ions or
112 neutrals. When plasma is confined in a micro zone, the collision rate increases significantly, as
113 well as the average energy exchanged. Therefore, reducing plasma size at constant pressure
114 leads to an increase of electron temperature. Secondly, due to the high surface-to-volume
115 ratio, the heat coupled from the power supply dissipates immediately and doesn't accumulate.
116 The non-equilibrium state provides new pathways for nanomaterial fabrication that cannot be
117 achieved by conventional ways and especially favors the synthesis of temperature sensitive
118 materials as well as the use of temperature sensitive precursors.

119 In order to get insights into the intricate features of microplasma, systematic diagnostic
120 studies of different types of microplasma have already been carried out. The parameters
121 characterizing microplasma feature such as the electron temperature T_e, electron energy
122 distribution functions (EEDFs), the electron density n_e and the gas temperature T_g have
123 been measured and calculated by various established techniques.

124 **Electron Temperature and Energy Distribution Functions**

125 The electron temperature, T_e, determines the energy of electrons in microplasma, while the
126 EEDFs reflect the distribution of energetic electrons. Both of them have a deep impact on

Table 2 Several experimental examples on the measurement of T_e

Power coupling	Gases	Discharge distance (μm)	Pressure (kPa)	T_e	n_e	Reference
DC	Ar	250	101.33	1 eV	10^{15} cm^{-3}	[87, 88]
DC couping 10 ns pulses	Ar	250	101.33	2.25 eV	10^{16} cm^{-3}	[87, 88]
DC	Xe	100	53.33	Increased more than an order of magnitude when coupling 20 ns pulses		[89]
DC couping 20 ns pulses	Xe	100	53.33			[89]
DC	Ne/ H$_2$	100	99.06	Confirm the presence of Ne$_2^*$ with T_e above 17 eV		[83]
DC	He/ H$_2$	250	80.00	Confirm the presence of He$_2^*$ with T_e above 20 eV		[84]
DC	Ar	600	40–93.33	0.9 ± 0.3 eV	10^{15} cm^{-3}	[85]

127 the process in nanomaterial synthesis. The high energy electrons enable efficient, non-
128 thermal dissociation of vapor precursors and other molecular gases to form reactive radical
129 species. The EEDFs allow the production of high concentrations of those species in a
130 certain T_e range. The higher electron temperature always leads to a rapid increase of
131 "effective" collision among the radicals and results in an enhancement of average energy
132 of them. As a consequence, more radicals for nanofabrication can be obtained during
133 ionization processes.

134 According to the researches on microplasma characterization, there are mainly two
135 factors affecting the non-thermal state of plasma: the non-transient effect and the micro
136 dimension, which can be adjusted by applying the pulsed discharges or by changing the
137 electrodes' distance. As mentioned above, the difference between the electron temperature
138 and gas temperature determines the plasma's non-thermal state. In this section the mea-
139 surement of the electron temperature are provided, along with a brief summary (Table 2)
140 and some representative examples on the two factors and the corresponding electron
141 temperatures [83–85], followed by a general statement of EEDFs in microplasma.

142 Normally the electron temperature could be measured by an optical emission spec-
143 troscopy or by the Thomson scattering based method. In the former one, the microplasma
144 is the source of an intense excimer emission. Through the line intensity measurements by
145 an optical emission spectroscopy the plasma electron temperature could be measured. In
146 the latter method, the free electrons of plasma accelerate and radiate in the oscillating field
147 under the effect of the high power laser, they have thermal velocity and cause the Doppler-
148 shift from the incident laser wavelength. By measuring the formed Doppler shifted scat-
149 tered spectrum, the electron temperature can be determined [86].

150 Frank and his co-workers [87, 88] measured the electron temperature in an Ar
151 microdischarge which was driven by a DC power supply. They found that the mean
152 electron temperature was about 1 eV, which was less than half of the value (about 2.25 eV)
153 when applying nanosecond pulses to the DC microdischarge. Another example is shown by
154 Moselhy et al. [89], they researched the Xe excimer emission in a DC generated
155 microdischarge by applying electrical pulses with 20 ns duration, and were able to increase
156 more than an order of the magnitude of the Xe excimer emission over a DC discharge,
157 which also indicated the existence of a significant fraction of high energy electrons in
158 microplasma. The raise of electron temperature when coupling pulsed discharge to the DC
159 plasma could be attributed to the electron heating effect, since it allows to heat electrons
160 while simultaneously keep the gas temperature unchanged.

161 As to the micro dimension, a typical example is using an Argon plasma sustained
162 between a capillary exit and a substrate (the distance can be changed) to study the rela-
163 tionship between the electron/gas temperatures and the micro dimension [82]. The results
164 showed that micro discharges exhibited the non-equilibrium characteristics. And reducing
165 the plasma size always leads to the increase of the electron temperature. Since the plasma
166 volume is reduced, a better power coupling from the electrical fields to the electrons could
167 be obtained, resulting in the increase of electron temperature. Electron temperature as high
168 as 14 eV could be achieved when the distance between the substrate and the capillary exit
169 was reduced to 0.2 mm.

170 In different microplasma conditions and configurations, the electron temperature varies
171 significantly from each other, so does the electron energy distribution. Although there are
172 no specific results on the relationship between EEDFs and other parameters, one common
173 result is that the electron energy distribution in microplasma is not following Maxwellian
174 distribution, which has already been verified by experimental studies [90] and simulations
175 [91].

176 A typical experiment was conducted between two parallel plate electrodes separated by
177 200 μm, which reflecting the electron and ion kinetics in atmospheric pressure He DC
178 microplasma [92]. In their experiments, various locations with different distances to the
179 cathode were investigated, and the EEDFs were tested. The results indicated that three
180 groups of electrons can be identified according to their energy: low energy electrons
181 (<1 eV), mild energy electrons (1–20 eV) and high energy electrons (>20 eV). Reflected
182 by the significant high energy tail attributed to the acceleration of electrons near the
183 cathode, the high energy electrons are abundant in this regime. In the bulk region, the high
184 energy tail disappears because the electric field is much lower than the sheath area. The
185 density of mild energy electrons also changes drastically with their energy, but is less than
186 the low energy electrons. This result proves again that the electron energy distribution
187 functions are not following the Maxwellian distribution.

188 ## Electron Density

189 Another important parameter to characterize microplasma is the electron density, n_e, which
190 varies significantly with the electrodes distance, pressure, power, gas component and so on.
191 Compared with conventional plasmas, microplasma can be operated at a higher pressure
192 due to the possible breakdown of "pressure times discharge distance" scaling, indicated by
193 the Paschen's law. As a result, the higher density energetic species such as electrons or
194 other charged particles can be obtained in microplasma. In nanofabrication process, the
195 high electron density can enhance the collision rates of precursors to produce high con-
196 centration of radical moieties, resulting in more efficient processes for the particle for-
197 mation and growth, especially highly favorable for the nanomaterial synthesis. In this
198 section the electron density measurement is introduced, along with some typical examples
199 of experimental parameters and the corresponding electron densities.

200 The electron density varies in different conditions, and it could be measured by the
201 Stark broadening technique or by the optical emission spectroscopy (OES) line-ratio
202 method. Experiment diagnostics demonstrate that the Stark broadening technique has a
203 fundamental limitation when the electron density is in the range between 10^{13} and 10^{16}
204 cm^{-3}. It is because the presence of resonance known as the van der Waals and the Doppler
205 broadenings, where the sum of low electron density may dominate the line broadening. The
206 OES line-ratio method is a good option when measuring the electron density in such a
207 range. While in the range of 10^{16}–10^{18} cm^{-3}, the Stark broadening technique is a better
208 alternative [93].

209 Many studies have been carried out to characterize the electron density of microplasma.
210 The results show that it differs largely in various setups, for example, the electron density
211 of glow discharge under atmospheric pressure was found in the region between 10^9 and
212 10^{13} cm^{-3}, in cases such as non-uniform discharges like atmospheric pressure micro-
213 plasma jet, this value could be between 10^{14} and 10^{15} cm^{-3} [81]. For the microwave
214 excited microplasma in argon near atmospheric pressure, the value could be more than
215 1×10^{14} cm^{-3}. The other factors, such as pressure, power, plasma dimension and oper-
216 ating gas also have an impact on the electron density.

217 Some general features have been observed in many unbounded microdischarges at
218 atmospheric pressure. A higher electron density will be obtained by operating at a narrower
219 discharge gap with a constant power. A higher power input will not change the electron
220 density but only lead to an expansion of the discharge volume [94, 95]. This is because the
221 small spatial size of plasma always has a relative large surface-to-volume ratio, resulting in
222 a relative high ionization degree, which is benefit for obtaining a higher electron density.

223 Generally the electron density was the highest at the middle of the discharge gap and
224 decreased along the way to each electrode. McKay et al. [96] researched various RF
225 atmospheric pressure He microplasmas with the frequencies ranging from 10 MHz up to
226 2.45 GHz, and found that the electron density was in the order of 10^{17} m^{-3} when the
227 electrodes were separated by a distance of 500 μm, and it varied in different positions.
228 However in bounded microdischarges, the electron density associates not only with gap
229 distance but also with input power. A RF (144.0 MHz) microplasma jet with different
230 powers was studied by J A Souza-Correa et al. [97], where the electron density increased
231 from 0.35×10^{15} to about 1.29×10^{15} cm^{-3} by increasing the power from 5 W to 50 W.

Gas Temperature

233 The gas temperature is another important parameter that must be considered in the process
234 of nanomaterial synthesis. A high gas temperature can result in coagulation and
235 spheroidization effects, leading to a significant thermal damage to the temperature sensi-
236 tive precursors, products or substrates involved, sometimes even cause the evaporation of
237 solid objects. This problem is more severe in microelectronic manufacturing industry
238 where the high gas temperature always easily exceed the melting points of some metallic
239 interconnects [1]. Microplasma is termed as the non-equilibrium low-temperature plasma
240 because the electron temperature is much higher than the neutral and ion temperature. The
241 non-equilibrium feature makes it a good choice for nanomaterial synthesis, especially for
242 temperature sensitive materials. In this section some interesting examples are provided,
243 along with the introduction of the gas temperature measurement.

244 There are normally two methods to measure the gas temperature in plasma. One is by
245 measuring the Doppler profile of emission or absorption lines, which is due to the velocity
246 distribution of atoms. Through the degree of Doppler broadening the translational tem-
247 perature can be determined [98], [99]. The $N_{2\ s}$ positive system can also be adopted to
248 estimate the gas temperature, according to the study of M. Bazavan et al. [100], the
249 electron temperature is generally much greater than the gas temperature, while the rota-
250 tional temperature is equal with the gas temperature. Therefore, by modeling the N_2
251 emission spectra of the molecular rotational bands belong to the N_{2s} positive system, the
252 rotational temperature in the microplasma can be obtained [100].

253 The gas temperature is in close connection with the discharge current and the gas
254 composition. Generally it is higher for molecular gases and lower for rare gases. The
255 pressure also has a significant impact on the temperature [101]. By observing the rotational
256 profile of the band of the second positive N_2 system in atmospheric pressure air micro-
257 plasma, the gas temperature was measured to range from 1700 to 2000 K when regulating
258 the discharge current from 4 to 12 mA [102, 103]. As to a microplasma generated in a
259 hollow cathode metal tube, the value was approximately 1200 K for pure Ar and kept
260 constant at different discharge currents. When nickelocene or copper acetylacetonate was
261 introduced to the plasma, the value was estimated to be 1200 and 1500 K at the current of 4
262 and 8 mA respectively [104]. Also the gas temperature depends strongly on pressure [105].
263 It increases from about 380 K at 50 mbar to around 1100 K at 400 mbar in the Ar
264 microplasma.

265 As can be seen from above, compared with conventional plasmas, microplasma has a
266 relatively higher electron temperature as well as a larger electron density, also its uniquely
267 featured non-equilibrium thermodynamics makes it particularly suitable for nanomaterial
268 synthesis. Besides, more potential applications in various fields are being studied and
269 investigated currently.

Microplasma Applications

271 Owing to its unique characteristics, a series of important, sometimes novel applications are
272 being exploited with the development of the microplasma technology, among which one
273 particularly promising and suitable application is for nanomaterial synthesis. Table 3
274 shows a comparison of some features valued by nanofabrication process between micro-
275 plasma and conventional plasma. A more detailed elaboration about the microplasma
276 application will be discussed in "Microplasma Configurations for Nanomaterial Fabrica-
277 tion" and "Nanomaterials Fabricated by Microplasma and Their Applications" sections.
278 Thanks to the high reactivity and relatively low operation cost, microplasmas have been
279 studied for the environmental application, especially for the destruction of the volatile
280 organic compounds (VOCs) such as ethylene, benzene, toluene and octane. Becker [106]
281 and his colleagues researched comprehensively on several types of microplasmas and their
282 use in the remediation of VOCs and biological decontamination. They obtained the
283 maximum VOCs destruction efficiency between 90 and 100 % for all researched com-
284 pounds. Takafumi Seto et al. [107] developed a miniaturized DBD microplasma device for
285 the decomposition of VOCs in the gas phase. The results showed that for a batch system
286 the toluene decomposition efficiency was almost 100 %, while for a flow system the
287 efficiency was more than 80 %.
288 A number of researches have concentrated on the use of microplasma for biological
289 systems. Since microplasma can inactivate microorganisms like cells, viruses, bacteria,
290 spores, biofilms, it has been used as a tool for inactivation, sterilization and bio-decon-
291 tamination [101, 106, 108]. Jerzy Mizeraczyk et al. [106] investigated an atmospheric
292 pressure microplasma generated by Ar and Ar/O_2 microwave for biomedical applications.
293 They performed several biocidal tests of samples treated by Ar, Ar/O_2 (0.5 %) and Ar/O_2
294 (1 %) microplasma, and found that there was a reduction of bacteria population for all
295 treated samples. Becker et al. [109] used capillary plasma electrode reactors in different
296 gas mixtures such as pure He, He/air, He/N_2 and air to study the inactivation of Bacillus
297 subtilis spores and Bacillus stearothermophilus spores. The results showed that the decimal
298 reduction factor (D-value, which is used to describe the time for reducing a specific active
299 microorganism concentration by one order of magnitude) could be achieved in less than
300 2 min.
301 Another interesting application is as an ultraviolet radiation source. Since the presence
302 of a high density of energy electrons in microplasma, it enables the excimer formation for
303 gases. Many researchers studied extensively on rare gases such as He [110], Ne [111], Ar

Table 3 Comparison between microplasma and convention plasma for features in nanofabrication processes

| Aspects	Microplasma	Convention plasma
Operating pressure	Atmospheric pressure	Always needs low pressure
Gas temperature	Can be as low as room temperature	Always needs temperature above 1000 °C
Particle size and distribution	Fine size, narrow size distribution	Relative larger size and wider size distribution
Setup and its investment	Quite small, easily moved, low cost	Always large, fixed, high cost

Plasma Chem Plasma Process
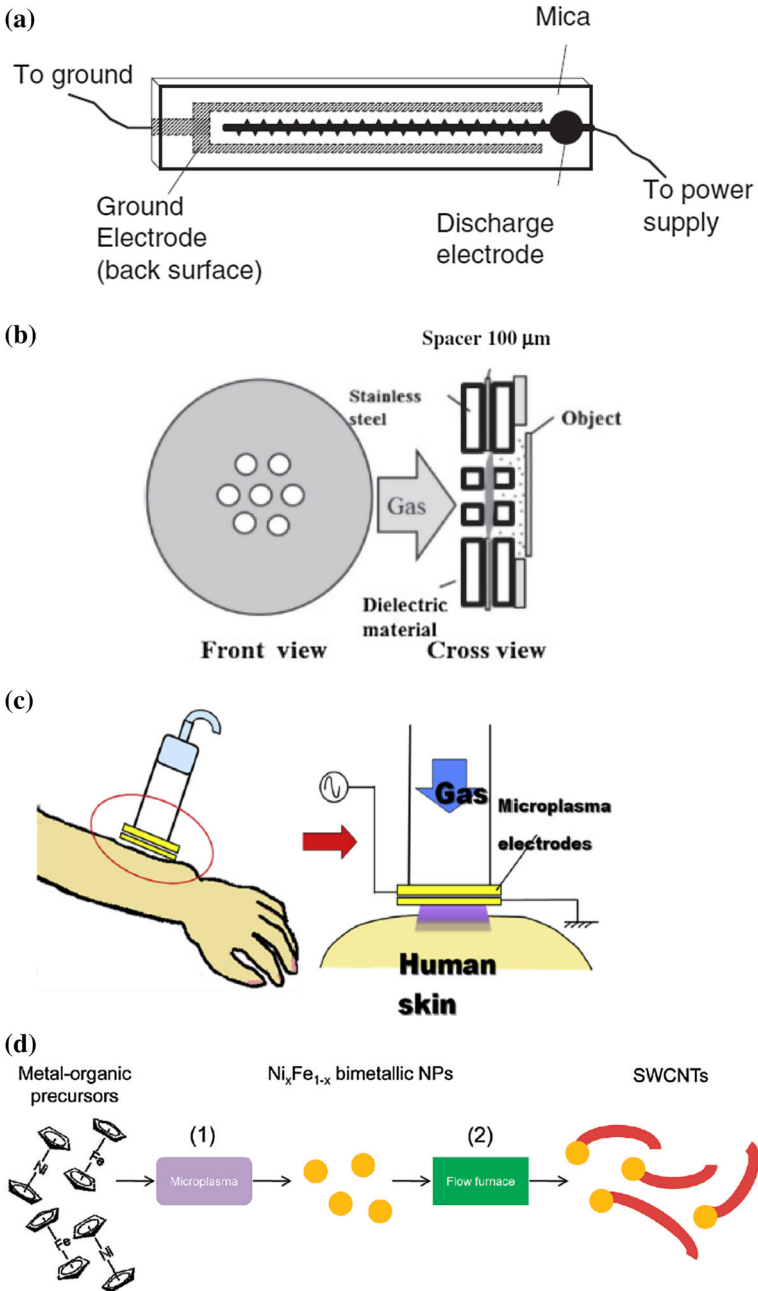
Fig. 1 Important applications of microplasma. **a** Destruction VOCs (reprinted with permission from [107], copyright 2005 The Japan Society of Applied Physics). **b** Surface treatment (reprinted with permission from [116], copyright 2012 The Japan Society of Applied Physics). **c** Surface sterilization treatment of human skin (reprinted with permission from [120], copyright 2014 Elsevier). **d** Synthesis of biometallic nanoparticles (reprinted with permission from [121], copyright 2009 American Chemical Society). **e** Ultra violet radiation sources (reprinted with permission from [122], copyright 2011 IOP Publishing)
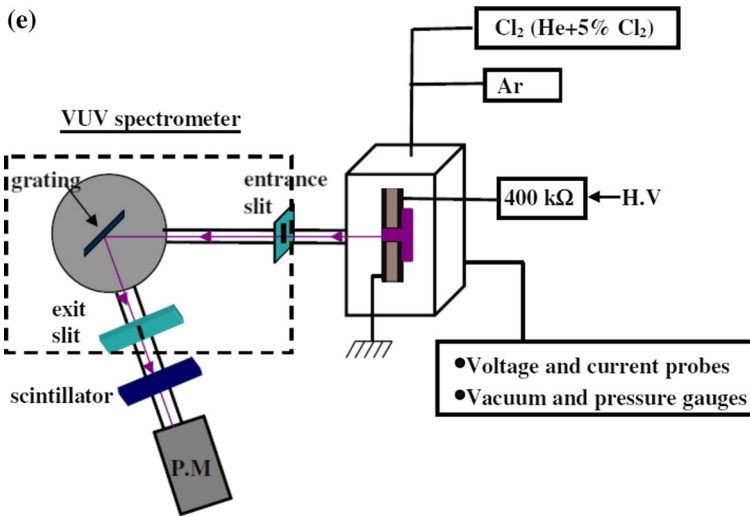
Fig. 1 continued

[112], Xe [113] or rare gas halide mixtures like XeCl [114], and concluded that up to 8 % internal efficiencies was approached by Xe excimer microplasma sources, while for heavier rare gases, lower efficiencies were achieved. As to the rare gas halide mixtures, efficiencies of the order of a few percent have been measured. With the advances in the design of microplasma arrays, there is a promising of using them as large area light sources both in visible and ultraviolet spectrums.

Microplasma has also been intensively studied for its application in surface treatment of glasses or polymers [115, 116]. In industries such as the display manufacturing, eye glasses and automobile side-view mirrors, hydrophilic property is required to make electrical connections between flat-panel surfaces, or to keep the glass surface transparent under mist conditions. As mentioned above, there are abundant active species and radicals in the microplasma environment, which can activate the molecules or atoms on the surface of glasses or polymers. With such interactions the surface will be modified and a hydrophobic layer could be formed to improve their hydrophilic property [117].

Other applications like biomedical diagnostics [118], spectroscopic analysis [119] and medical treatment of human skin [120] were also reported and under development. Figure 1 illustrates several important applications of microplasma that have been reported in recent years [107, 116, 120–122].

Microplasma Configurations for Nanomaterial Fabrication

So far various microplasma configurations have been developed and used in different applications. Generally the classification could be made based on the power sources, ranging from DC power supply to other different kinds of radio frequency from kHz to GHz. Also it could be classified by different electrode geometries, such as dielectric barrier discharges (DBDs) [123], hollow electrode discharges [124], micro-cavity discharges

328 [125], microplasma jets [126], microplasma arrays [127] and so on. Figure 2 shows several
329 microplasma systems with different electrode geometries.

Hollow-Electrode Microcharges

331 Hollow-electrode microcharges are relatively simple structures used for nanomaterial
332 fabrication and can be operated stably at atmospheric pressure and room temperature.
333 Generally there are two hollow metal capillary tubes separated by 1–2 mm, both are
334 connected to a DC power supply and act as the cathode and the anode respectively.
335 Meanwhile, they also function as the precursor transporters, in which precursor vapors are
336 introduced by a flow of inert gas such as Ar or He, and dissociated in the plasma area
337 between two electrodes. The formed aerosol particles can be collected by an electrostatic
338 precipitator or by a filter installed after the reactor. In an emblematical hollow-electrode
339 microcharge, the typical voltage and current used to prepare nanomaterials are at the level
340 of hundred V and several mA, which are too small to ionize electrodes. Therefore, elec-
341 trodes won't take part in the reactions.
342   In a representative structure developed by Chiang and Sankaran [128], microplasma was
343 formed between two electrodes which were separated by 2 mm. The cathode was a
344 stainless steel capillary tube with an inner diameter of 180 μm, the anode was a stainless
345 steel tube/mesh, and both were sealed inside a quartz tube to keep stable plasma operation.
346 During the discharge process, the size and distribution of the generated nanoparticles could
347 be measured by the followed aerosol size classification. In addition, they used the produced
348 nanoparticles as catalysts for carbon nanotubes (CNTs) growth in a tube furnace, and
349 studied catalytic properties of various compositionally-tuned Ni_xFe_{1-x} nanoparticles. The
350 two-stage microplasma system is schematically illustrated in Fig. 3.
351   A similar microplasma reactor as Fig. 3 was used to produce multimetallic nanoparti-
352 cles by the dissociation of organmetallic vapors [129]. The organmetallic compounds such
353 as $Ni(Cp)_2$, $Fe(Cp)_2$, $Cu(acac)_2$, $Pt(acac)_2$ were used, and a series of mono-, bi-, and tri-
354 metallic nanoparticles with various compositions were synthesized by varying the flow rate
355 of precursors. Ultra-fine (less than 5 nm in diameter) nanoparticles with narrow size dis-
356 tribution could be fabricated because of the extremely short residence time (about 1 ms) in
357 such micro-structure.
358   In addition to preparing metal nanoparticles and CNTs, hollow-electrode microcharges
359 were also used to prepare Si nanowire [104] or nanodiamonds [130]. The results showed
360 that this novel approach could produce ultrafine nanoparticles at atmospheric pressure and
361 room temperature.

Microplasma Jets

363 Currently various configurations of microplasma jets were proposed and used as nano-
364 material fabrication tools, with different types of power supplies (dc, rf or microwave) to
365 ignite and sustain the plasma. Gas jets with external electrodes, like wire electrode or tube
366 electrode, were built. Belmonte et al. [81] pointed out that the following three items should
367 be addressed concerning microplasma jets: (1) Controlling the location of the deposition
368 area by regulating the precursors' flow - currently the most common way is locating
369 capillaries where the precursors flow through. (2) Managing consumable wires that were
370 used as nanomaterial sources - most of the microplasma jets use the consumable wires as
371 precursors of the to-be-built nanostructures; the wire is consumed as the reaction goes on.
372 (3) Coupling the power supply (dc, rf or microwave) to the system to form plasma - the
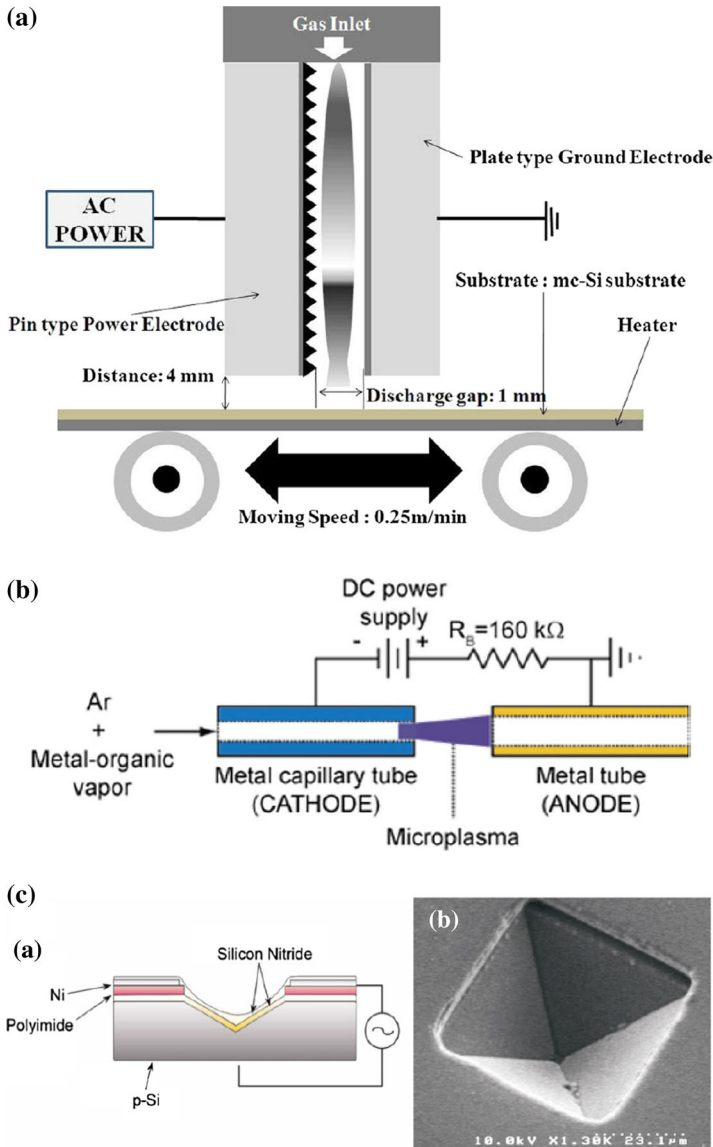
(a)

(b)

(c)

Fig. 2 Different types of microplasma systems classified by electrode geometries. **a** DBD microplasma (reprinted with permission from [123], copyright 2005 IOP Publishing). **b** Hollow electrode discharges (reprinted with permission from [124], copyright 2010 IOP Publishing). **c** Microplasma jet (reprinted with permission from [126], copyright 2006 Elsevier). **d** Micro-cavity discharges (reprinted with permission from [125], copyright 2006 IOP Publishing). **e** Microplasma arrray (reprinted with permission from [127], copyright 2014 Macmillan Publishers Ltd)

373 power supply has strong influence on the growth of nanomaterials, and various approaches
374 were adopted based on the configuration of setup. Several representative examples of
375 microplasma jets are shown in Fig. 4. Based on whether to use consumable wires as
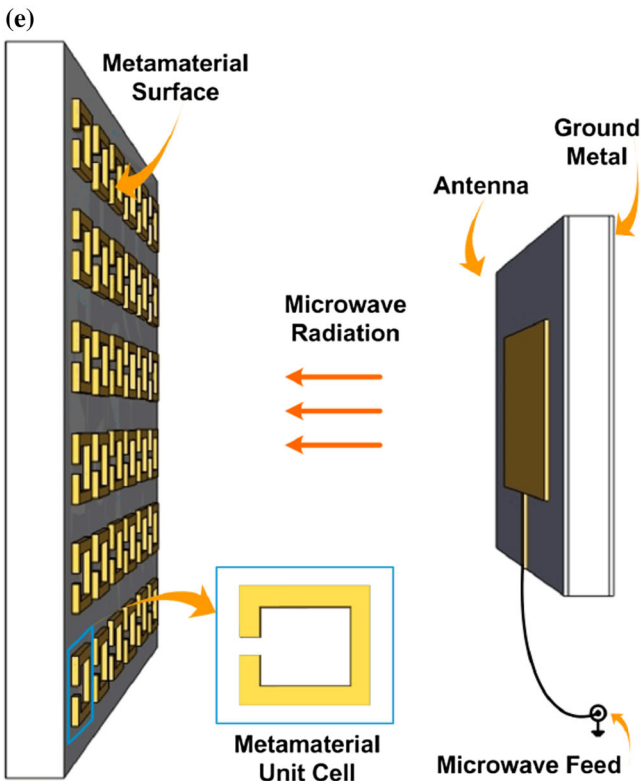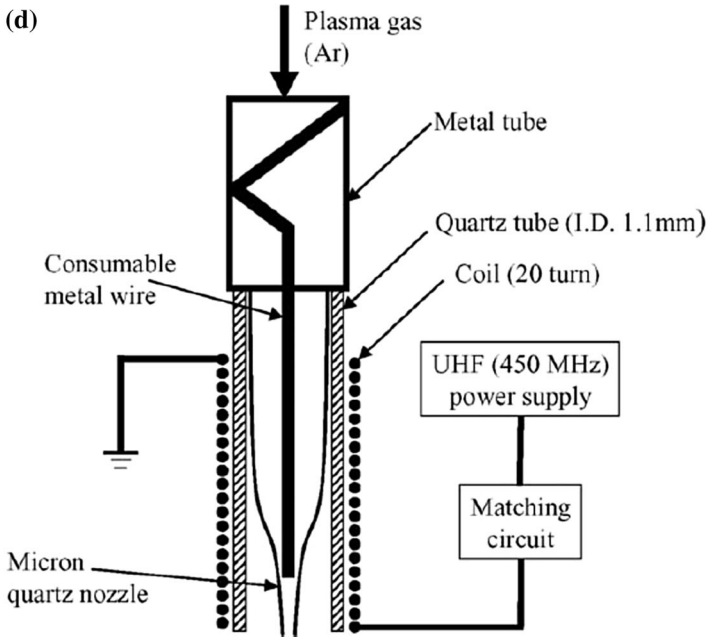376 electrodes or not, there are two categories of microplasma jets.

Plasma Chem Plasma Process
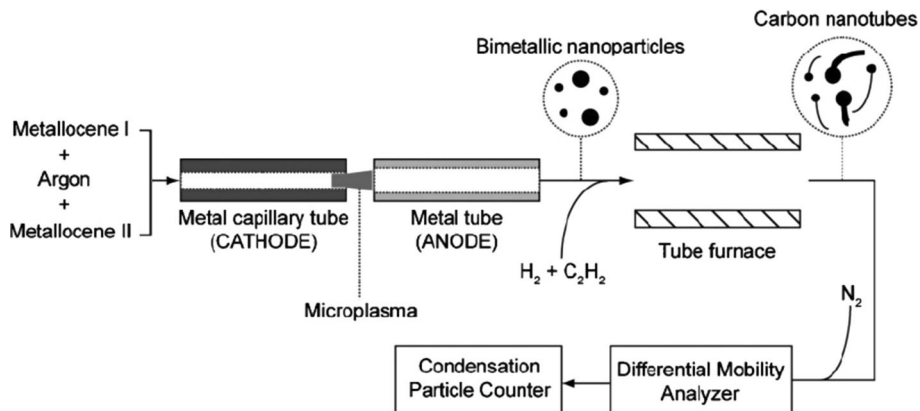
(d)

(e)

Fig. 2 continued

Fig. 3 The two-stage hollow-electrode microcharges. Reprinted with permission from [128], copyright 2008 Wiley-VCH

Microplasma Jets with Consumable Wires as Electrodes

As mentioned above, the consumable wires were used as precursors in many microplasma jets. Therefore, metal wires such as W [126, 131], Fe [126], Cu [126], Mo [79, 132–134] and Au [135] were reported to be used for preparing desired nanomaterials. Table 4 summaries the main reports using consumable wires for nanomaterials preparation.

Generally the microplasma jets using consumable wires as electrodes were quite similar in their configurations. Usually a metal wire was used as the solid precursors and inserted inside a capillary tube. Various plasma gases such as Ar, He, N_2, H_2, O_2 or their mixtures flew through the capillary tube to form the plasma. According to the different ways of coupling the power supply, microplasma could be formed inside or outside the tube. A part of the metal wire resided within the microplasma volume, and reactions would take place on its surface. In such a configuration, different nanomaterial structures could be obtained on the wire surface or on the substrate below the plasma jet [136]. During the deposition process, process parameters such as the gas flow rate, gas composition, substrate distance and input power can be varied to produce a wide range of nanomaterial structures. The
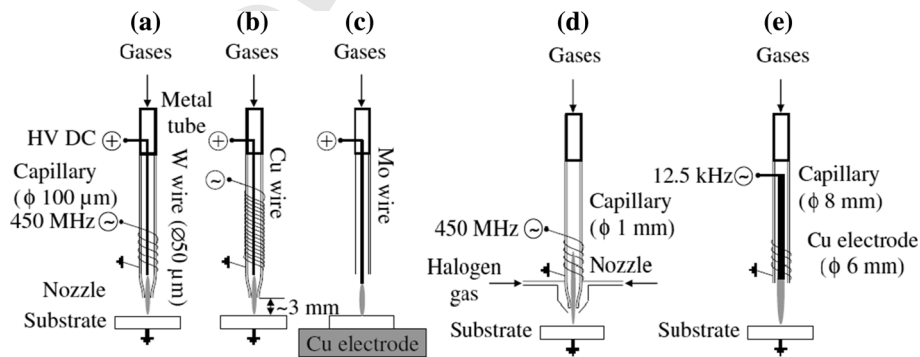

Fig. 4 Representative examples of microplasma jets. Reprinted with permission from [81], copyright 2011 IOP Publishing

392 results showed that this approach is a cost-effective and versatile way to produce metal/
393 metal-oxide nanomaterials compared with other methods.
394   A representative configuration is shown in the Fig. 4c [133]. A Mo wire (100 μm
395 diameter) was used as the precursor as well as the electrode and connected to a high
396 voltage power supply (5 kV). A Si substrate was placed above the copper electrode and
397 used for the collection of nanomaterials. Ar and O_2 mixtures were introduced during the
398 deposition process. Ignited by a high voltage pulse, microplasma was sustained between
399 the Mo wire tip and the Si substrate by an ultrahigh frequency (450 MHz) power supply,
400 finally the MoO_x nanomaterials could be obtained.

401 *Microplasma Jets with Tubes/External Electrodes*

402 There are also reports using tubes or external electrodes instead of the consumable wires to
403 form plasma jets. In that case, extra precursors such as CH_4 [137, 138], $SiCl_4$ [139],
404 $Ti[OC_3H_7]_4$ [140, 141], $Pd(hfac)_2$ [142] and $Cu(hfac)_2$ [142] are provided to prepare the
405 desired products. Table 5 summaries the main reports using tube or external electrodes to
406 prepare nanomaterials by microplasma jets.
407   Compared with the microplamas using consumable wires as electrodes, this type of
408 microplasma jet has a higher degree of flexibility in configuration. Since there are more
409 available ways to couple the power supply to the system, a wider range of process
410 parameters could be set, like precursors ratio, power coupling mode, residence time and so
411 on. Furthermore, in addition to metal/metal-oxide nanomaterials, this method can also
412 produce other nanomaterials by dissociating corresponding precursors, making it possible
413 to prepare more products with different structures.
414   One typical example of the microplasma jet with tube electrodes is shown in Fig. 5
415 [143]. A hollow WC tube was used as the cathode electrode and Ar carrier, and connected
416 to a RF (13.56 MHz) power supply via a matching circuit. During the experiments, a
417 microplasma jet was formed at the tip of the WC tube and contacted directly with a Fe-
418 coated Si substrate. CH_4 was supplied to the microplasma jet through a separate gas line. In
419 this research, variables such as the plasma exposure time, plasma power, gas flow rate and
420 composition were studied. By plasma heating, a mixture of CNTs, Si nanowires and Si
421 nanocones were produced via the combination processes of $FeSi_x$ catalytic growth, Si
422 diffusion and oxidation. Another example was using a hollow microneedle as the electrode
423 by connecting it to an AC power supply [137]. After introducing He and the precursor - gas

Table 4 Microplasma jets using consumable wires as electrodes to prepare nanomaterials

Metal wires	Plasma gas	Power supply	Structures	References
Mo wire, d = 100 μm	Ar + 2 % O_2, 20 sccm	UHF (450 MHz), 20/31 W	MnO_X-NPs, NSs	[79, 132–134]
Au wire, d = 100 μm	Ar + 4 % H_2, 200 sccm	UHF (450 MHz), 0.8 W	Au-NPs	[135]
W wire, d = 50/ 100 μm	Ar + 1 % O_2, 5–40 sccm	UHF (450 MHz), 20 W	WO_X-NPs	[126, 131]
Fe wire, d = 100 μm	Ar, 0.5 sccm	UHF (450 MHz), 20 W	Fe-NPs, NSs	[126]
Cu wire, d = 100 μm	Ar, 30 sccm	UHF (450 MHz), 20 W	Cu-NSFs	[126]

NPs nanoparticles, *NSFs* nanostructure films, *NSs* nanostructures

424 mixtures of CH_4 and H_2, microplasma was ignited by applying 100 W RF power. Com-
425 pared with CVD method, a higher CNTs deposition rate could be achieved by this method
426 even at a lower temperature. This may attribute to the plasma effect which lowered the
427 activation barrier of CNTs growth.

428   A representative example of microplasma jet with external electrodes is a similar
429 structure as the Fig. 4a [144]. A tungsten wire was inserted in a quartz tube and connected
430 to a high DC power supply. A copper coil surrounding the quartz tube acted as the external
431 electrode. Microplasma was ignited by a DC power supply (15 kV) and sustained at
432 atmospheric pressure with the external electrode. CH_4 and Ar were used as the precursor
433 and the carrier gas to form carbon materials without extra heating. Another similar
434 microplasma jet with external electrodes was applied to deposit TiC, TiO_2 and TiN
435 coatings [140]. Plasma was generated in a SiO_2 nozzle, which was wounded by a copper
436 wire as the external electrode. By using titanium tetraisopropoxide as the precursor, tita-
437 nium-based nanomaterials were deposited on stainless steel rods to improve their
438 performance.

439   Considering the scaling-up of microplasma jet system, Cao et al. [145] studied a ten-jet
440 microplasma array (Fig. 6) for its electrical and optical characteristics, and found that it
441 had achieved excellent uniformity jet-to-jet both in time- and space-wise. If microplasma
442 arrays could be properly designed and used in the process of nanomaterial synthesis, it may
443 allow to increase nanomaterials throughput drastically and to enable the deposition of thin
444 films in a relatively large area.

Table 5 Microplasma jets with tube/external electrodes to prepare nanomaterials

Precursors	Plasma gas	Power supply	Structures	References
CH_4, H_2	He, 30 sccm	RF (15–35 kHz), 100 W	CNTs	[137]
CH_4	Ar + 0.5 % CH_4, 200 sccm	UHF (450 MHz), 5–30 W	C–NSs	[144]
Fe-coated Si, CH_4	Ar/CH_4, 50/50 sccm	RF (13.56 MHz), 35 W	Si–NCs, CNTs	[138]
$SiCl_4$	Ar + 0.8 % H_2, 200 sccm	UHF (144 MHz), 35 W	Si–NCs	[139]
Ti[OCH(CH$_3$)$_2$]$_4$	Ar + 0.1 % CH_4/N_2, 200 sccm	UHF (430 MHz), 10 W	TiC/TiN–NSFs	[140]
Ti[OCH(CH$_3$)$_2$]$_4$, O_2	He, 490 sccm O_2, 10 sccm	RF (13.56 MHz), 12 W	TiO_2–NSFs	[141]
Pd(hfac)$_2$, Cu(hfac)$_2$, Ni(Cp)$_2$, O_2	Ar, 100–300 sccm O_2, 10–100 Torr	DC, 1–20 mA, 500–700 V	CuO/PdO/NiO–NSs, NSFs	[142]
CH_4, H_2	CH_4, 10 sccm; H_2, 350 sccm	RF (14 MHz)	CNTs	[188]
CH_4	Ar, 10–50 sccm; CH_4, 10–50 sccm	RF (13.56 MHz), 40 W	CNTs, CNWs, Nanodiamond	[197]
Fe-coated Si, CH_4	Ar, 10–50 sccm CH_4, 10–50 sccm	RF (13.56 MHz), 35 W	CNTs, Si-NCs, Si–NWs	[143]

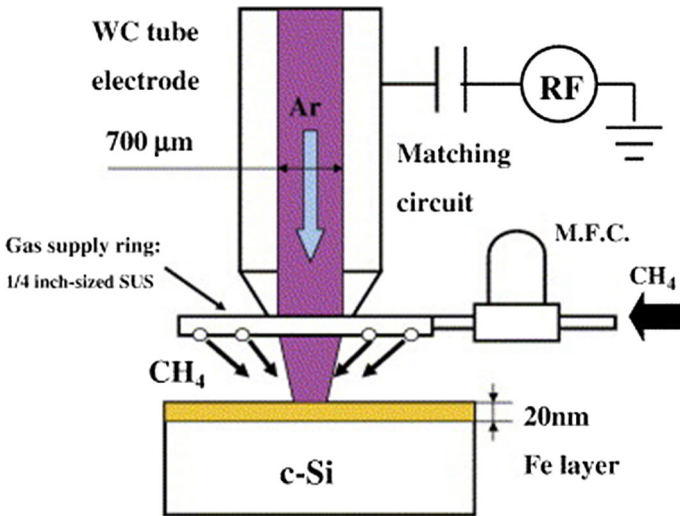*NPs* nanoparticles, *NW* nanowires, *NSFs* nanostructure films, *NSs* nanostructures, *NCs* nanocrystals

Fig. 5 Schematic diagram of microplasma jet with a WC tube as cathode. Reprinted with permission from [143], copyright 2007 Elsevier

Microtorches

Plasma torches have been wildly used for the synthesis of nanomaterials, particularly suitable for the deposition of coatings with different performance. In most cases, gas temperatures are above 4000 K, which are close to thermal equilibrium state [81]. The high
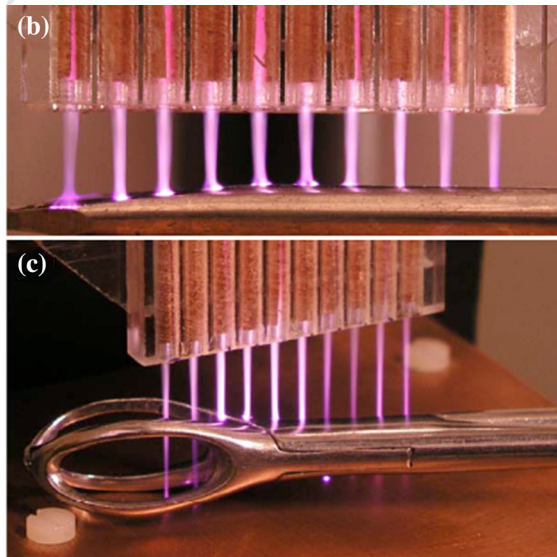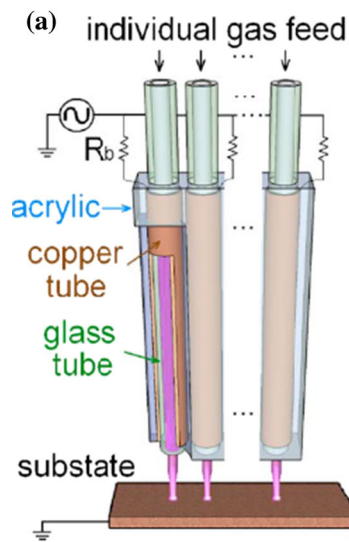

Fig. 6 The photograph of an array of microplasma jets setup. Reprinted with permission from [145], copyright 2009, AIP Publishing LLC

449 temperature and high energy density of the plasma torch make it possible to spray
450 refractory materials, which can't be achieved by other plasma methods. The produced
451 nanoparticles are easily clogged under such high temperatures, leading to a broad size
452 distribution. Plasma torches can be generated by microwave or dc arc discharge, which are
453 shown in Fig. 7 [81]. It is worthwhile to mention that they are contamination free since
454 they could be formed without any internal electrodes.

455 When the plasma torch is confined in a relative small spatial zone, it becomes "micro-
456 torch". Seriously speaking, there is no clear boundary between plasma torch and micro-
457 plasma torch. However, compared with microplasma jets, the plasma formed in micro-
458 torch commonly has a larger zone and a higher gas temperature, and the produced
459 nanomaterials always have larger sizes and a wider size distribution.

460 Precursors fed to microplasma torches are mainly solid or liquid. Clogging in the small
461 discharge space should be avoided. For DC microplasma torches there are usually two
462 approaches to introduce the precursors, as illustrated in Fig. 8 [81]. One approach is
463 feeding precursors perpendicularly to the microplasma torch but not in contact with any
464 electrode, as shown in Fig. 8a. In the other case, precursors could be feed axially flowing
465 through inner electrodes, as shown in Fig. 8b. When a microplasma torch is applied for the
466 deposition of various performance coatings, the coatings properties are mainly influenced
467 by two factors-the particle velocity and the particle temperature [146]. To improve the
468 quality of microplasma sprayed coatings, one effective way is to inject precursors axially
469 along the plasma torch, allowing a longer dwelling time for precursors in the plasma zone.
470 However, the sprayed particles may adhere to electrodes in such case, limiting the practical
471 application of DC microplasma torches. Since microwave torches do not have internal
472 electrodes, the blocking problem can be avoided.

473 As mentioned above, temperatures in microplasma torches are usually very high, par-
474 ticularly suitable for producing refractory material coatings, or handling refractory pre-
475 cursors. However, they are unfriendly for high quality nanoparticle synthesis, especially
476 the heat-sensitive materials. And the particles produced by microplasma torch always have
477 a relatively broader size distribution and are easier to agglomerate compared with the other
478 microplasma methods. In order to prevent particle agglomeration and to improve the
479 product quality, a quenching section becomes necessary, which helps to obtain particles
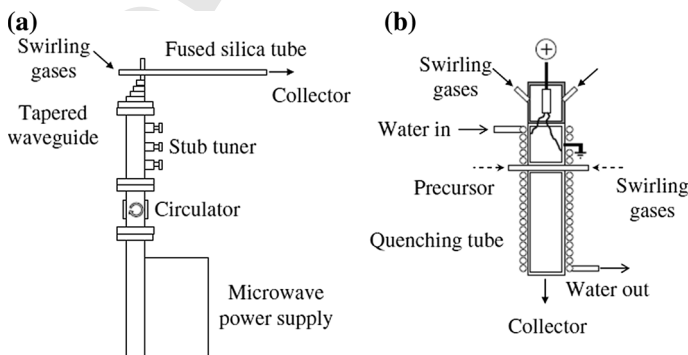480 with reduced size distribution. Other methods such as adding extra electrical field,

Fig. 7 Microplasma torches generated by **a** microwave discharge and by **b** dc arc discharge. Reprinted with permission from [81], copyright 2011 IOP Publishing

481 confining plasma volume or reducing residence time could also be helpful to obtain high
482 quality products.
483   One typical example of producing refractory nanomaterial coatings is using a hollow
484 cathode microplasma torch to deposit Al_2O_3 coating [146], in which commercially
485 available Al_2O_3 powder with a size distribution from 10 to 20 μm was used as the pre-
486 cursor. Argon acted as both the operating gas and the carrier gas during the deposition
487 process. Different plasma powers were used to deposit Al_2O_3 films, which were obtained at
488 a 10 mm spray distance on a steel plate used as the substrate. The results revealed that
489 almost the Al_2O_3 particles in the coating were well-flattened, and the particle thickness
490 would decrease with the increase of plasma power.

491 ## Liquid Phase Microplasma

492 A range of approaches to generate microplasmas on/in the liquid have been developed,
493 such as applying the DC power sources, high frequency power sources, pulsed high voltage
494 power supplies and several other methods. Generally the liquid phase microplasma can be
495 classified into two categories, the noncontact glow charge electrolysis (GDE) and the
496 contact glow charge electrolysis (CGDE) [147]. In the former one, plasma is formed in the
497 gas phase that above the solution surface, while in the latter case plasma is formed inside
498 the solution. Anyhow, the plasma and the liquid interface is a ighly complex area where
499 multiple phases (gas, liquid and vapor) exist. Moreover, charged or highly reactive species
500 such as gaseous and solution ions, electrons and radicals make the liquid phase micro-
501 plasma of promising applications in various fields. One particularly interesting application
502 is for nanomaterial synthesis [148].
503   It's a new and attractive way to produce colloidal nanoparticles in an aqueous solution,
504 where the microplasma is spatially located, and the bulk liquid still remains at the ambient
505 condition. As we know, the liquid density is much larger than the gas density. Moving the
506 plasma to the liquid phase allows the increasing of pressure more significantly than the gas
507 phase plasma, resulting in an additional confinement of the plasma [80]. The highly
508 confined and localized discharges may offer potential routes for preparing nanomaterials
509 directly and efficiently. Furthermore, a lot of active chemical species can be generated in
510 aqueous phase, including OH·, O·, H·, H_2O_2 and O_3, which are beneficial for nanofabri-
511 cation. There are also studies showed that the water may contribute to the non-equilibrium
512 state of microplasma. As well known, a fraction of the energy in plasma that coupling to
513 the electrons could heat up the bulk gas. In liquid plasma, water acts as a heat sink, the heat
514 can be quickly dissipated, thus it could prevent the gas temperature from drastic increase
515 and preserve a non-equilibrium state [149].
516   For nanomaterials synthesized by the GDE method, one example was demonstrated by
517 Huang et al. [150], in which they produced Ag nanoparticles via a microplasma-assisted
518 electrochemistry process (Fig. 9a). A capillary SS tube acted as the cathode and was placed

Fig. 8 Two main approaches to introduce precursors to DC plasma torches. Reprinted with permission from [81], copyright 2011 IOP Publishing
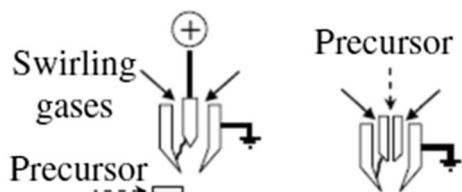
519 2 mm above the surface of electrolyte. Helium was coupled as the operating gas and
520 formed the plasma between the cathode and the electrolyte surface. A Pt foil was used as
521 the anode and placed 3 cm away from the cathode, a DC power supply with a high voltage
522 around 2 kV was applied to ignite the plasma. They synthesized Ag nanoparticles with
523 various sizes and dispersions by controlling different process parameters. After that, they
524 prepared Au nanoparticles in $HAuCl_4$ solution by a similar setup, which is schematic
525 shown in Fig. 9b [151]. A SS capillary and a Pt foil acted as the cathode and the anode
526 respectively, with He as the plasma gas. Au NPs were synthesized at the interfacial region
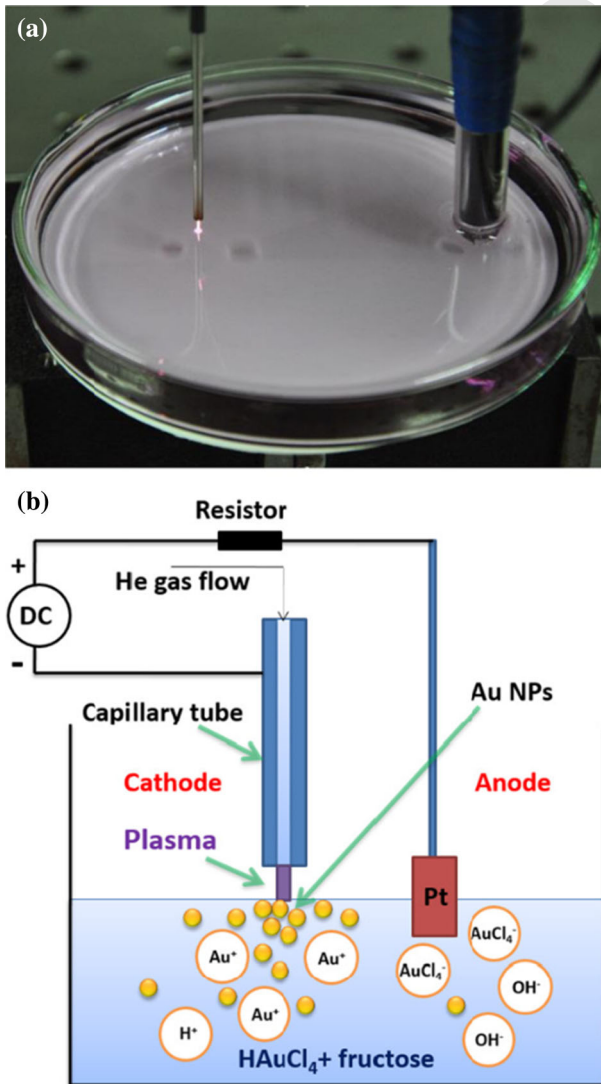527 where the formed plasma interacted with the solution. They found the size of Au NPs was a

Fig. 9 The GDE experiment setup (**a**) and its schematic (**b**) for preparing Au nanoparticles. Reprinted with permission from [151], copyright 2014 Springer

528 function of process parameters, such as solution temperature, current, and rate of stirring.
529 In addition to the metal nanoparticles, the GDE method were also applied to produce
530 metal-oxide nanoparticles such as Fe_3O_4 [152] and Cu_2O [153].

531 For nanomaterials prepared by the CGDE method, one typical example was demon-
532 strated in Fig. 10, in which Au nanoparticles of different shapes were fabricated in aqueous
533 solutions [154]. Tungsten electrodes were separated by 0.3 mm and put in a vessel filled
534 with $HAuCl_4$ solution, while the temperature was maintained at 25 °C by a cooling system.
535 The plasma was ignited by a pulsed DC power supply with a frequency of 15 kHz. During
536 the discharge process, applied voltages of 1600 and 3200 V were used. The solution was
537 stirred by a magnetic stirrer, with sodium dodecyl sulfonate as a stabilizer. By this
538 approach, Au nanoparticles around 20 nm in diameter with exotic shapes such as trian-
539 gular, pentagonal or hexagonal were obtained.

540 A novel technique was used to prepare water-soluble CNTs by a setup based on the
541 CGDE technology (Fig. 11) [155]. The microplasma was generated between two elec-
542 trodes by applying high pulsed voltage. O_2, Ar and N_2 were used as the bubbling gases to
543 enhance the discharges between electrodes. Commercial CNTs were added in deionized
544 water, and the formed suspensions were treated by the microplasma. After one hour's
545 treatment in a stirred tank, high water-soluble CNTs were obtained. The study showed that
546 the high energy electrons of the microplasma could enhance the excitation and ionization
547 of H_2O molecules and lead to the generation of radicals such as O· and H·. Then the
548 strongly oxidative O· reacted with H· to form OH· groups at the CNT surface, and the
549 introduction of hydrophilic OH· groups to the CNT surface caused a higher solubility of
550 CNTs in water.

551 There is a general agreement that the liquid phase microplasma would provide a
552 potential guidance for various applications, such as the nanoparticle synthesis [150], flame
553 electrochemistry [156], spectrochemical analysis [157], wastewater remediation [158] and
554 so on. However, the underlying mechanism of reactions is still poorly understood, and the
555 chemical and electrochemical processes still remain unclear. Currently just several kinds of
556 nanoparticles have been produced by this method, such as Au [151], Fe_3O_4 [152], Cu_2O
557 [153], Ag [148, 159], Cu [160], Ti [161]. In some ways the current state of liquid phase
558 microplasma is still considered as an "art" rather than a "precise science" [147], more
559 investigations are needed to get those confusions solved.

Fig. 10 The CGDE experiment setup for preparing Au nanoparticles. Reprinted with permission from [154], copyright 2008 American Vacuum Society
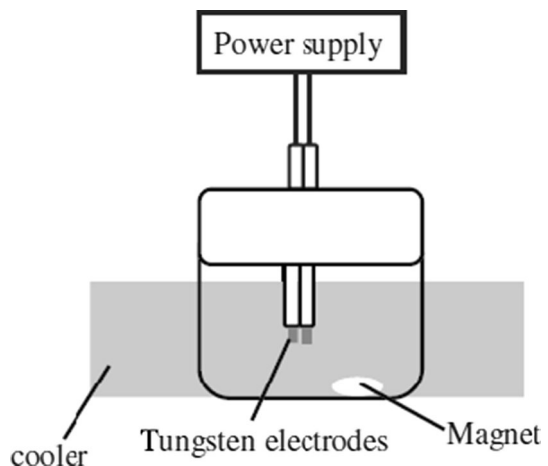
Selection of Appropriate Microplasma Configuration for Nanomaterial Synthesis

The selection of microplasma configuration mainly depends on the precursors and the desired products. One benefit of microplasma is its micro-geometry. Therefore, the required quantity of precursors is quite small compared with other methods, which inevitably associates with low product output. It should be pointed out that the application of microplasma on nanomaterial synthesis may only be cost-effective for producing high value-added products or products that can't be produced by other means.

For the hollow-electrode microcharges, the electrodes also function as the "precursor carriers". Owing to their small inner diameters, the solid or liquid precursors are not allowed to be used directly in such configurations, because they can easily block the tubes. Therefore, nanomaterials can only be synthesized by the gas-phase nucleation from their precursor vapors. If a precursor is in solid or liquid state, the most common way is using another gas (often plasma gas, such as Ar, He and N_2) to carry its vapor to the reaction zone. If a precursor has a low vapor pressure at room temperature, the heating tape or oven can be adopted to get the desired value.

For microplasma jets and microtorches, the option for precursors has more flexibility. In principle, liquid, gas or solid can be used as precursors, although in most cases gas or solid state precursors are chosen as they are easy to handle in such configuration. There is even a report about using supercritical CO_2 as the precursor to produce carbon materials by a DBD microplasma jet [162], which shows that supercritical fluid could also serve as an
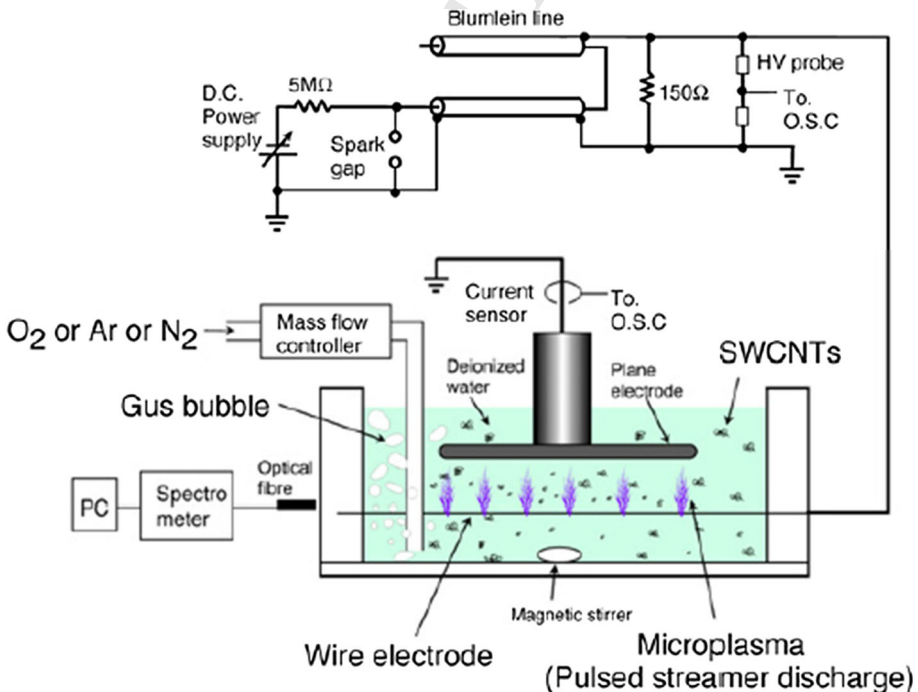

Fig. 11 Schematic experiment setup for preparing water-soluble CNTs. Reprinted with permission from [155] copyright 2007 IOP Publishing

581 alternative precursor and provide a favorable environment for nanomaterial synthesis.
582 Another attractive concept to supply precursor is evaporating or sputtering a sacrificial
583 metal electrode, correspondingly metal nanostructures or metal oxides can be prepared,
584 which can't be approached by other microplasma configurations. However, as mentioned,
585 the temperatures of microtorches are usually very high, which may lead to a thermal
586 damage to precursors that are temperature sensitive. In such cases, it's better to choose
587 microplasma jets rather than microtorches. On the other hand, if the spherical nanoparticles
588 are to be prepared, the microtorches are best suited, because the droplet-like nanostructures
589 are expected to be the prominent shape in high temperatures [1].

590   The precursors of liquid phase microplasma are quite different from that of other kinds
591 of plasma, and almost are electrolytes containing metal ions of the desired nanomaterials.
592 By such device, the salts with low vapor pressures are especially suited as precursors. In
593 addition to the metal salts, sacrificial metal electrodes are also used as precursors, which
594 are oxidized to form metal ions in the solution and then reduced to metal nanoparticles by
595 the impact of plasma. Compared with traditional electrochemical methods which need
596 organic stabilizer to prevent the agglomeration or the deposition of nanoparticles on
597 electrodes, this approach is stabilizer-free because of the free-contact of electrolytes with
598 electrodes.

599   Above all, Table 6 shows a brief summary of precursors used and products obtained by
600 the above mentioned microplasma configurations. It can be used as a guideline for process
601 design or for choosing an appropriate type of plasma in nanomaterial synthesis.

Nanomaterials Fabricated by Microplasma and Their Applications

603 Since nanomaterials exhibit unique properties that are attractive to various high perfor-
604 mance applications, currently the nanomaterial fabrication is considered as one of the most
605 promising research fields. Microplasma is particularly suitable for nanomaterial fabrication
606 thanks to its unique characteristics, such as the non-equilibrium state, stable operation at
607 atmospheric pressure and room temperature, high radical densities. It can dissociate pre-
608 cursors efficiently and nucleate nanoparticles from atomic level, allowing preparing

Table 6 A summary of precursors used and products obtained by different microplasma configurations

Microplasma configuration	Precursors	Ever reported products
Hollow-electrode microcharges	Gas, liquid or solid, but liquid or solid should use their vapors	Metal NPs or alloys, Si nanostructures CNTs, nanodiamonds, etc
Microplasma jets	Gas, liquid, solid or supercritical fluids, especially suitable for metal wires	Metal NPs or oxides, carbon or Si nanostructures, diamond nanostructures
Microtorches	Gas, liquid or solid, but not suitable for temperature sensitive precursors	Spherical metal NPs or oxides
Liquid phase microplasma	Metal salts or metal wires, especially suitable for metal salts with low vapor pressures	Metal NPs like Au, Ag, Ni, Ti, and Cu
		Metal-oxide NPs like Fe_3O_4, Cu_2O

609 nanoparticles below 10 nm in size through the so-called "bottom-up" way. Different
610 configurations of microplasma setups have been developed, with a wide range of nano-
611 materials synthesized in recent years.

Metallic Nanoparticles

613 Metallic nanoparticles could be synthesized by a variety of methods, for example, using
614 microfluidics in single-phase flows or multi-phase flows, additive-assisted synthesis, car-
615 bothermic reduction and so on. Metallic nanoparticles prepared by microplasma were
616 already mentioned in "Microplasma Configurations for Nanomaterial Fabrication" section,
617 the reaction mechanism and their application will be further introduced in this section.

Synthesis and Mechanism

619 As introduced in "Hollow-Electrode Microcharges" section, Chiang et al. [128] synthe-
620 sized Fe and Ni nanoparticles from ferrocene and nickelocene respectively by a hollow-
621 electrode microplasma system. The obtained nanoparticles were narrowly dispersed and
622 non-agglomerated compared with other methods. Bimetallic and multimetallic nanopar-
623 ticles were also synthesized in such microplasma system, such as Ni_xFe_{1-x} [128], $Ni_{0.47-}$
624 $Cu_{0.53}$, $Ni_{0.18}Cu_{0.82}$, $Ni_{0.22}Fe_{0.29}Cu_{0.49}$, and $Ni_{0.34}Fe_{0.46}Cu_{0.20}$ [129].
625 　The existence of high density energetic electrons in small scale reaction zones allows
626 the decomposition of precursors and the nucleation of nanoparticles efficiently in situ.
627 Currently the detailed mechanism for nanoparticle nucleation and growth in microplasma
628 is still unclear. The process may have something to do with precursors' concentration,
629 dissociation enthalpy or other processing parameters. However, a general hypothesis of the
630 mechanism can be shown in Fig. 12 [129]. Organometallic compounds like $Ni(Cp)_2$,
631 $Fe(Cp)_2$ and $Cu(acac)_2$ vapors are dissociated in microplasma to form radical moieties such
632 as Ni·, Fe·, Cu· and C_5H_5· as the first step. Afterwards, these radicals collide with each
633 other randomly to nucleate pure metal NPs or multimetallic NPs.
634 　Metal nanoparticles such as Ag [148], Au [151], Cu [160] and Ti [161] that prepared by
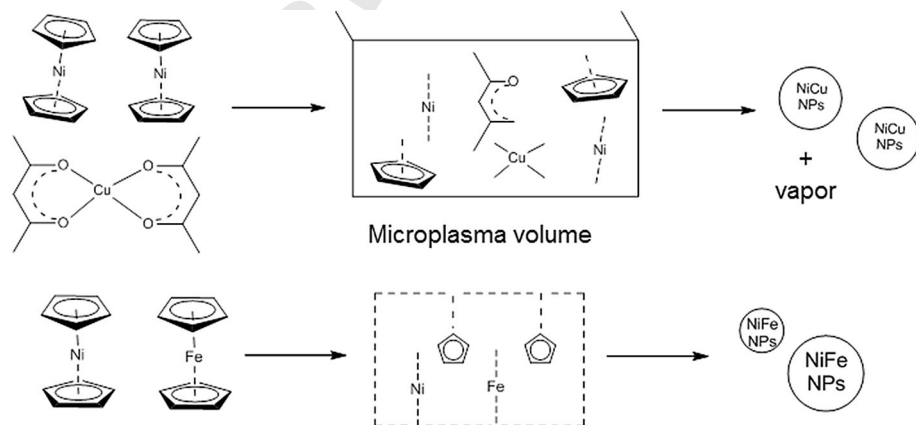635 microplasma electrochemical method were introduced in the "Liquid Phase Microplasma"

Fig. 12 The assumed mechanism of pure metal NPs and multimetallic NPs synthesis by microplasma. Reprinted with permission from [128] copyright 2011 Wiley-VCH

636 section. A potential mechanism for the nucleation of metal nanoparticles M from deduction
637 of metal cations M^+ via GDE approach is shown in Fig. 13 [147]. Similar to the con-
638 ventional electrochemical processes, there are three distinct reasons for ion transportation
639 to the plasma–liquid interface: (1) electric field induced metal ions (M^+) migration, (2)
640 convection, (3) diffusion. In electrolytes the convective force is weak and only attributes to
641 the free convection. There is no appreciable concentration gradient in the electrolytes
642 except the plasma–liquid interface. As a result, the diffusion dominates only in this area.
643 Once M^+ reaches the interface, they undergo electron transfer process to produce metallic
644 M^0 atoms. However, because of the inability to characterize the plasma–liquid interface by
645 electrochemical probes, the mechanism of electron transfer process and nanoparticle
646 nucleation still remains unclear. Once M^0 atoms are obtained at the interface, they may
647 serve as sites for nanoparticle nucleation and growth. Afterwards, the formed nanoparticles
648 may aggregate and become large clusters or networks, then transported to electrolyte bulk
649 by diffusion or convection process.

650 *Applications*

651 Metallic nanoparticles attracted immense interest in a wide range of fields such as the
652 catalysts [128, 159], biological applications [163], medical applications [164], bio-sensing
653 applications [165] and so on. In this section two typical examples are introduced, one is for
654 CNTs growth and another for cancer treatment, corresponding to nanoparticles production
655 by the gas phase microplasma and by the liquid phase microplasma respectively.
656 Metallic nanoparticles produced by microplasma can be used as catalysts for many
657 processes, for example, Ni and Fe nanoparticles show excellent catalytic activity for CNTs
658 growth [166]. Chiang et al. [128] used Ni and Fe nanoparticles to catalyze the CNTs
659 growth. The results showed that the reduction of Ni nanoparticle, with the size distribution
660 from 3.1 nm to 2.2 nm, caused an improvement for the rate of CNTs growth by 13 times.

Fig. 13 The potential
mechanism for preparing metal
nanoparticles by GDE approach
[147]. Reprinted with permission
from [147], copyright 2013
American Vacuum Society
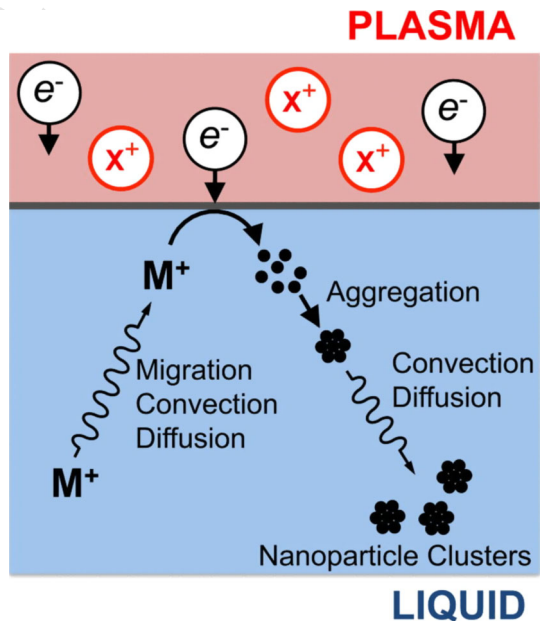
661 Moreover, Ni nanoparticles with different dimensions could control precisely the CNTs'
662 inner and outer diameter as well as wall numbers [167]. Afterwards, they studied the
663 catalytic activity of the bimetallic nanoparticles, and found that Ni_xFe_{1-x} could signifi-
664 cantly increase the catalytic activity and lower the activation energies for CNTs growth
665 compared with monometallic nanoparticles [128]. For example, with $Ni_{0.67}Fe_{0.33}$
666 nanoparticles, the CNTs could grow at 300 °C with activation energy as low as 37 kJ/mol,
667 while CNTs only grew at 400 °C with Ni nanoparticles and the activation energy was
668 estimated to be 73 kJ/mol.

669 Metallic nanoparticles, particularly the noble metal nanoparticles, showed promising
670 prospects in cancer treatment due to their unique characteristics such as the high surface to
671 volume ratio, facile surface chemistry, excellent optical properties as well as the ability to
672 convert radio frequencies or light into heat [164]. They can extravasate into tumor stroma
673 and accumulate at tumor sites, and be tracked directly by optical microscopy because of
674 their special optical and imaging properties. Furthermore, the noble metal nanoparticles
675 hold great promise to kill cancer cells selectively through hyperthermia effect. Micro-
676 plasma electrochemical method may become the most attractive and reliable way to pre-
677 pare metal nanoparticles for biological application, since it is environment friendly without
678 any stabilizers, the products are smaller with narrower size distribution compared with the
679 products achieved by other methods.

680 **Si Nanomaterials**

681 *Synthesis and Mechanism*

682 Silicon nanoparticles were synthesized in microplasma driven by the RF power supply
683 [138, 168] or DC power supply [104, 169] at atmospheric pressure, through different
684 microplasma configurations. Silicon tetrachloride ($SiCl_4$) and silane (SiH_4) are the most
685 commonly used precursors.

686 The Si NPs synthesized by RF microplasma jet were spherical and without any
687 agglomeration [168], shown in Fig. 14. They were highly crystalline with the size smaller
688 than 5 nm. Besides, it was proved that Si NPs could be nucleated and grown at temper-
689 atures well below their crystallization threshold, which was attributed to the effective
690 heating in the non-thermal microplasma. Another example is to synthesize the Si NPs by
691 using SiH_4 as the precursor and Ar as carrier gas, a hollow-electrode microdischarge was
692 used to produce high quality Si nanoparticles [170, 171]. The results showed that blue
693 luminescent Si nanoparticles with diameters in the range of 1–3 nm and with narrow size
694 distribution could be obtained by this method. In addition, when H_2 was introduced in the
695 plasma, a lower possibility of Si condensation and a lower particle growth rate were
696 achieved, owing to the enhanced surface passivation of Si by hydrogen [172].

697 Although the detailed mechanisms are different in various processes, usually the general
698 mechanism follows a similar rule. Taking SiH_4 as an example [80, 170–172], silane
699 dissociation takes place by electron impact dissociation and allows the formation of dif-
700 ferent kinds of reactive radical species such as SiH· and H·, which were confirmed by their
701 emission lines in the OES spectra. The addition of H_2 not only promotes the particle
702 heating but also induces a transition of Si from amorphous state to crystalline state.
703 Afterwards, due to their high reactivity, the formed radicals such as SiH_3·, SiH_2·, H· collide
704 and react with each other immediately to nucleate clusters via the recombination process.
705 More and more radicals collide with those clusters, and they will grow or agglomerate by
706 additional radical or vapor deposition on their surface or by the collisions with other

707 clusters to form Si nanoparticles. Due to the fact of the short residence time and being
708 charged, the particles agglomeration was suppressed, products with very good size control
709 were obtained in the gas phase, which can be collected in the followed sections.

710 *Applications*

711 Si is one of the most abundant elements on earth, and is well known for its significant
712 application in the semiconductor industry. However, the indirect band gap of Si elements
713 causes the poor optical properties, limiting their application in many fields. Recently the
714 nanostructured Si materials have spurred intense interests and are the most popular
715 functional materials in commercial electronic industry due to the following reasons: (1)
716 good stability and non-toxicity; (2)quantum confinement effects; (3) well-established
717 fabrication technique; and (4) high carrier mobility [173]. It is an inspiring direction to use
718 Si based nanomaterials to explore a diverse of application fields.
719 Among the silicon nanostructures, Si nanowires are the low-dimensional nanostructures
720 which have unique structural, optical, electrical and thermoelectric properties [173, 174].
721 They have a direct band gap because of the quantum confinement, therefore, they are
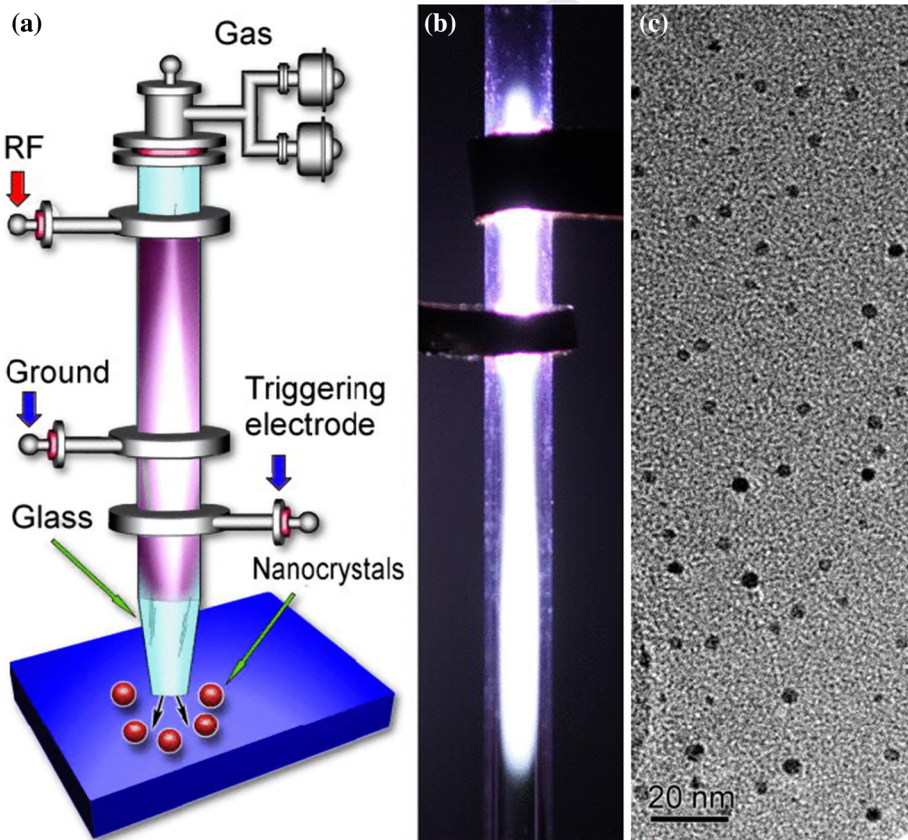

Fig. 14 Plasma setup (**a**, **b**) and the produced Si NPs (**c**). Reprinted with permission from [168] copyright 2014 AIP Publishing LLC

722 optically active materials suitable for photonics applications [175]. Besides, the excellent
723 light-trapping properties of Si nanowires make them the low-cost and high-efficient
724 alternatives of the traditional silicon solar cells, because they allow the orthogonalization
725 of light absorption [176]. Besides, when they were used as lithium ion batteries' anodes,
726 they exhibit superior electrochemical performance along with good recyclability and sta-
727 bility [177]. Furthermore, with the high selectivity and sensitivity, the label-free detection
728 capability and real-time response, Si nanowires have shown promising prosperous in
729 cellular recording and biomedical diagnosis applications [178].

730 **Metal-Oxide Nanomaterials**

731 *Synthesis and Mechanism*

732 Various microplasma configurations and processes have been developed to produce metal-
733 oxide nanomaterials. Currently the most common configuration is the microplasma jet
734 (Fig. 4), because it is convenient to use sacrificial metal electrodes as precursors, or use
735 tube/external electrodes with flexible precursors, allowing many approaches to couple
736 power supply to ignite and sustain the plasma.
737 MoO_x nanoparticles were prepared by an atmospheric pressure microplasma jet (similar
738 to Fig. 4 (c)) using a consumable Mo wire as the electrode. Two possible mechanisms were
739 proposed based on the gas flow rates (Fig. 15) [132]. When the gas flow rate was less than
740 20 ml/min, the reaction and condensation effect of active species is dominant. The atomic
741 oxygen can oxidize Mo wire surface easily, once it was oxidized the molybdenum oxides
742 volatilize into gas phase. Then under the impact of ions and electrons, volatilized oxides
743 were decomposed into Mo· and O· in the microplasma, and these radicals react and
744 condense with each other to form Mo oxides. However, at a higher gas flow rate, the gas
745 temperature was reduced, and the molybdenum wire surface was in a molten state, leading
746 to the ejection of molten droplets to form Mo oxides NPs downstream. Therefore, the
747 difference of mechanism is that in low gas flow rates atomic oxygen is used to oxidize both
748 Mo· and Mo wire surfaces, while in high gas flow rates it is consumed only to oxidize Mo
749 wire.
750 In addition to consumable wires, organometallic precursors such as nickelocene,
751 Pd(hfac)2 or Cu(hfac)2 hydrate were also used as precursors. The metal oxide nanowires
752 such as CuO, PdO and NiO were produced at different conditions [142]. There was also a
753 report which was using a pulsed microplasma cluster source to synthesize metal oxide
754 films by ablating metallic targets. Nanostructured Mo, W, and Nb oxide films with several
755 hundreds of nanometers thickness were formed by this approach [179].
756 Different mechanisms were proposed for metal-oxide nanoparticles produced by
757 microplasma jets. However, generally in every process microplasma plays two important
758 roles [142]: (1) it dissociates precursors and provides active metal species directly, from
759 which nanomaterials nucleate and grow; (2) it interacts with background gas to provide
760 active oxygen species, which are an essential part of metal oxides nanomaterial synthesis.
761 For different processes, specific mechanisms vary largely because reactions in micro-
762 plasma are so complicated, since they are closely related to the type of precursors, gas flow
763 rates, temperatures as well as other plasma parameters.
764 As mentioned in "Liquid Phase Microplasma" section, metal-oxide nanomaterials like
765 Cu_2O and Fe_3O_4 also can be produced by the GDE method. Compared with microplasma
766 jet, the setup of liquid phase microplasma is much simpler, because all the nanoparticles
767 can be collected in solution instead of substrates. Furthermore, it doesn't need to provide
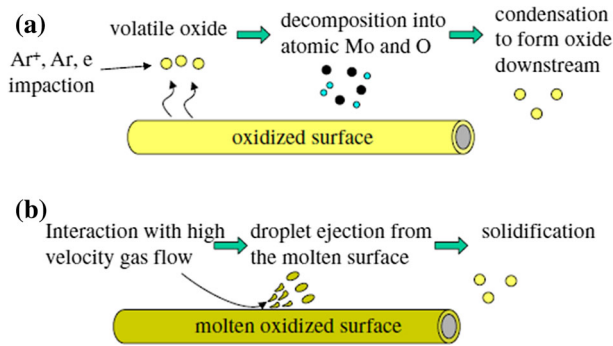
Plasma Chem Plasma Process

Fig. 15 Mechanisms of Mo oxides synthesis in **a** low gas flow rates and **b** high gas flow rates. Reprinted with permission from [132], copyright 2006 IOP Publishing

768 O_2 as the precursor, for O· can be achieved from H_2O. However, only DC power supply
769 has been reported to sustain the liquid phase plasma, while for microplasma jet, various
770 alternatives such as RF or microwave power supply systems have been reported.

771 *Applications*

772 Metal oxide nanostructures have the potential to play an important role in many tech-
773 nologies, such as the sensing devices [180], biomedical applications [181], energy con-
774 servation [182], catalysis [134], waste water treatment [183] and so on. On account of their
775 unique mechanical and chemical properties, metal oxide nanomaterials are favored as the
776 functional coating materials in various fields. This section just focuses on a promising
777 field—the deposition of functional metal oxides coatings by microplasma. Some repre-
778 sentative examples of functional nanomaterials will be introduced, followed by the
779 potential way to deposit the large scale coatings using microplasma arrays.

780 Metal oxide nanomaterials with different performances are considered to be perfect
781 coating materials in many applications. For example, TiO_2 coated surface is hydrophilic
782 and remain transparent under mist or rainwater because the contact angle between water
783 and surface is small. There is hardly any water drop deposited on the coated surface. Such
784 coatings could be used for eyeglasses or automobile side-view mirrors [184]. Al_2O_3
785 nanomaterial is an ideal coating material which is very attractive for the metal cutting
786 industry because of its favorable chemical stability, excellent thermal property, great wear
787 and deformation resistance, together with its super toughness [185]. Cu_2O nanomaterials
788 recently have received significant attentions as alternatives for Si nanomaterials in trans-
789 parent conduction films, which are attributed to their excellent optical absorption properties
790 [186]. Mo oxides coatings have also been widely used in a wide range of engineering fields
791 due to their high melting point, excellent corrosion resistance as well as beneficial
792 mechanical property, making it possible to control the friction and wear performance of
793 materials over a wide range of temperatures [187].

794 High quality functional coatings could be obtained by microplasma technology. Com-
795 pared with other methods, microplasma can produce ultra-fine nanomaterials with high
796 uniformity. The coating process can be conducted in gas phase by the direct plasma
797 jet/torch spraying or in liquid phase by the plasma electrochemical method. However,
798 because of its relatively low output, one key unanswered question of microplasma

799 technology is whether it can provide required throughout for industrial coating applica-
800 tions. With the growing demanding for high quality functional coatings in various fields,
801 there is an increasing need for the deposition of large area coatings. A novel idea holding
802 great promise for large scale deposition was proposed by adopting microplasma arrays (a
803 typical example was shown in Fig. 6 [145]), which can increase material output easily via
804 arranging series of microplasmas together and operating them simultaneously. Moreover,
805 microplasma arrays also have the potential to deposit more than one layer coatings with
806 different performance when using a two-dimensional design, which is depicted in Fig. 16
807 [80]. Operated with different precursors and conditions in each array, multilayer func-
808 tional coatings can be obtained by scanning microplasma arrays in one direction. Therefore, if
809 microplasma arrays were well designed, with appropriate precursors and processes,
810 functional metal oxides coatings could be prepared in large scales by this approach.

811 **Carbon Nanomaterials**

812 *Synthesis and Mechanism*

813 A series of carbon nanomaterials were prepared by microplasma technology in past years,
814 including the CNTs [128, 137, 166, 188], nanodiamonds [130, 189], nanorods [188],
815 carbon nanoparticles [190] and so on. In this section, several typical examples were
816 introduced.
817 One smart microplasma system for producing nanodiamonds at atmospheric pressure
818 and room temperature is using the hollow-electrode microcharge configuration (Fig. 3)
819 [130]. Ethanol vapor was chosen as the carbon source and continuously introduced to the
820 microplasma by Ar and H_2 mixture. A glass filter was installed at the exit of aerosol flow to
821 collect nanoparticles. The results confirmed that high-purity nanodiamonds could be pre-
822 pared at relatively neutral conditions by this route. Although the detailed mechanism has
823 not been discussed yet, it was confirmed that the existence of C2 and CH· species during
824 the dissociation process would contribute to the nucleation of solid carbon clusters and
825 nanodiamonds respectively. The introduction of H_2 was affecting the diamond growth and
826 the non-diamond carbon etching, resulting in the stabilization of diamond phase carbon and

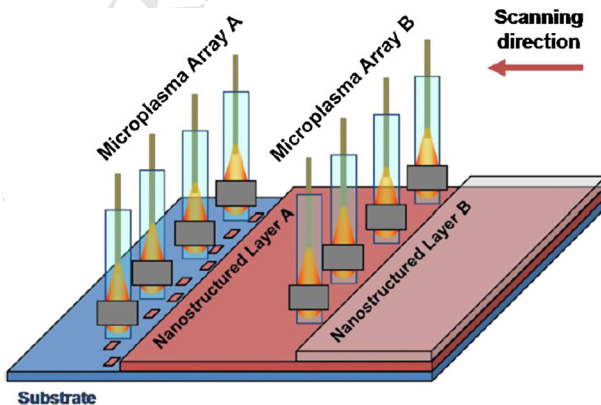**Fig. 16** Two-dimensional microplasma arrays for the deposition of multilayer coatings [80]. Reprinted with permission from [80], copyright 2010 IOP Publishing
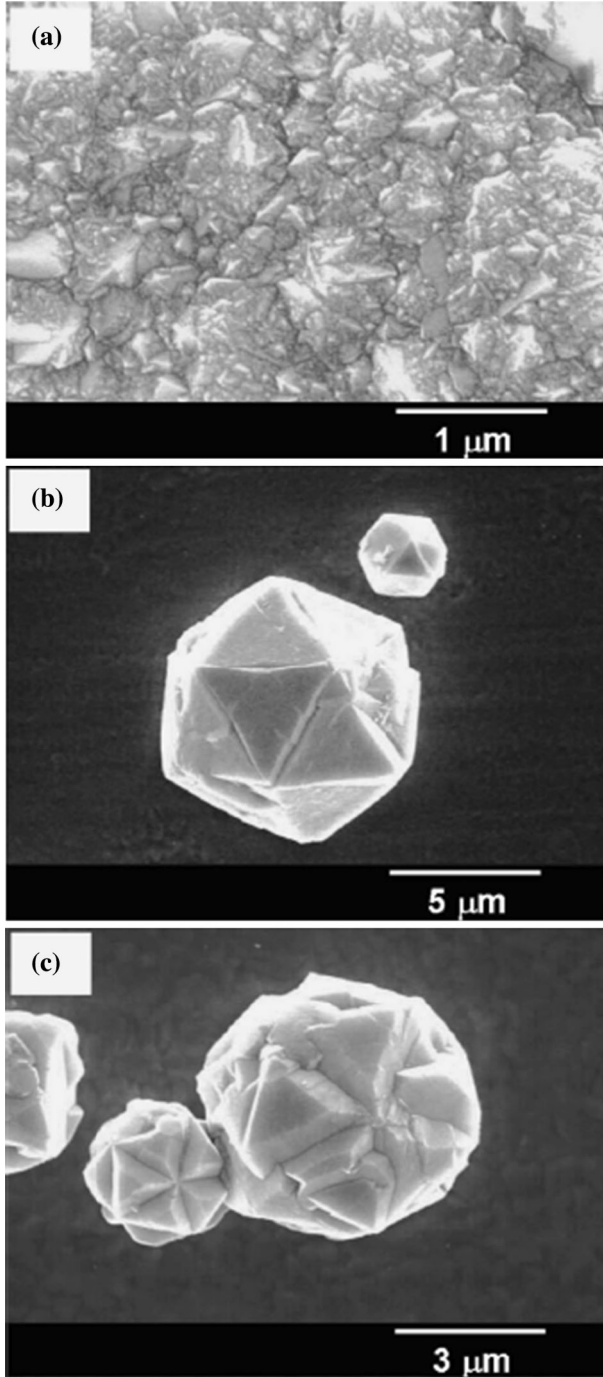
Fig. 17 Diamond film and nanocrystals produced by microplasma jets at various CH_4 concentrations. **a** 0.5 % CH_4, **b** 0.25 % CH_4, **c** 0.1 % CH_4. Reprinted with permission from [189], copyright 2002, AIP Publishing LLC

827 the selective removal of non-diamond phase carbon. Another example about the deposition
828 of nanodiamond crystals was achieved by a microplasma array [189], in which four jets
829 were operated in parallel in the capillary tubes. The deposition process was conducted at a
830 sub-atmospheric pressure (200 Torr) chamber, with H_2 and CH_4 as precursors. Molyb-
831 denum foils were adopted as substrates and kept at 800 °C during the process. The results
832 showed that the high quality diamond nanocrystals could be prepared at various CH_4
833 concentrations (Fig. 17).

834 A pin-electrode microplasma configuration was used to prepare carbon nanomaterials in
835 a SEM chamber, where a Pd needle was used as the anode and a Si wafer coated by Pt films
836 was used as the cathode [190]. CH_4 was adopted as carbon source and a pulsed high
837 voltage power supply operated at 10 Hz frequency was used to sustain the plasma. Various
838 carbon nanomaterials such as the CNTs, carbon nanoparticles or carbon nanosticks were
839 obtained at different deposition times in this process.

840 The mechanisms are quite different in the processes of carbon nanomaterials synthesis,
841 which are closely associated with deposition parameters such as the input power, gas
842 composition, substrate temperature, catalyst, gas flow rate, etc. Generally they undergo a
843 similar rule, the chemical bonds of carbon sources are broken by the impact of energetic
844 electrons in microplasma. The precursors are dissociated into various radicals. These high
845 reactive radicals collide with each other to nucleate small clusters and form nanomaterials
846 after a series of complex processes.

847 One interesting phenomenon observed during carbon nanomaterial synthesis by
848 microplasma is the self-organization. Nanomaterials prepared in plasma are always
849 charged and interact with each other under Coulombic forces and van der Waals forces,
850 allowing the formation of well ordered, large scale nanostructures [80]. An example
851 system was using a stainless steel pipe as the electrode and a Ni wire as the substrate, in
852 which vertically aligned CNTs were deposited on the Ni wire surface when a negative bias
853 voltage was applied on it [188]. The studies showed that a large quantity of species such as
854 $CH_3\cdot$, $CH_2\cdot$ and $CH\cdot$ could be obtained in the plasma. With the negative bias voltage, a
855 perpendicular static electric field was formed on the Ni substrate, resulting in the formation
856 of vertically aligned CNTs bundles. Another example is the formation of self-organized
857 carbon nano-connections between the catalyst particles when exposed to a microplasma jet
858 [191]. In the experiment, CH_4 and Ar were introduced to form the plasma which was
859 sustained by a UHF (450 MHz) power supply. A Si substrate coated by Ag or Fe was
860 treated by this plasma. After the depositing process for a certain time, self-organized
861 carbon connections were produced. The results suggested that the electric field determined
862 the growth direction of carbon nano-connections. In this case the catalyst particles were
863 dispersed over the substrate surface and created a two dimensional electric field. Between
864 these two adjacent catalytic nanoparticles the electric field gradient was maximum along
865 the straight line, which significantly affected the carbon surface diffusion and growth
866 process. Therefore, compared with vertically aligned CNTs formed due to the electric field
867 perpendicular to substrate, carbon nano-connections grew along the surface in virtue of the
868 electric field along the substrate surface.

869 *Applications*

870 The carbon nanomaterials have attracted enormous interest for many potential applications
871 due to their extraordinary properties. For example, nanodiamond has superior hardness,
872 high thermal conductivity and chemical stability, so it is used as an excellent composites
873 for filler materials [192]. With the addition of nanodiamonds to the polymers, substantial

874 improvements in mechanical strength, thermal conductivity, adhesion and wear resistance
875 can be obtained. Besides, they are non-toxic, biocompatible and have tunable surface
876 chemistry, particularly suitable for biomaterials in the bone tissue engineering [193]. CNTs
877 are also widely used for their superior mechanical properties. For example, they were
878 adopted as reinforcement materials for polymer composites [167], implant materials [194]
879 and scaffolds for cell encapsulation [195]. Furthermore, their high thermal conductivity
880 makes them attractive as the cooling system materials on computer chips [196]. Increas-
881 ingly potential applications will be explored and achieved in future with the developing
882 technology of producing high-quality carbon nanomaterials at low cost.

Conclusions and Outlook

884 This review paper has studied the recent achievements on microplasma as an innovative
885 tool for functional nanomaterial synthesis. The unique physical and chemical properties
886 caused by the increased surface-to-volume ratio and the decreased electrode spacing are
887 the main reasons that make microplasma particularly suitable for nanomaterials synthesis.
888 Various microplasma systems were designed to fabricate nanomaterials. And the
889 nanometer-sized, high purity and narrow size distributed products were synthesized by this
890 unique approach.

891 Despite the promising perspective of microplasma technology, some challenges remain.
892 Investigations on the mechanisms are highly required to better understand the process for
893 nanomaterial generation. And the universality of microplasma technology for different
894 nanomaterial synthesis should be further studied. The further development to an indus-
895 trialization level of microplasma technology would require the intensive collaboration
896 among material chemists, physicists, electrical engineers and chemical engineers.

References

1. Ostrikov K, Xu SY (2007) Plasma-aided nanofabrication. Wiley-VCH, Germany
2. Wang Q, Shi H, Yan B, Jin Y, Cheng Y (2011) Steam enhanced carbon dioxide reforming of methane in DBD plasma reactor. Int J Hydrog Energy 36(14):8301–8306
3. Wang Q, Cheng Y, Jin Y (2009) Dry reforming of methane in an atmospheric pressure plasma fluidized bed with Ni/γ-Al$_2$O$_3$ catalyst. Catal Today 148:275–282
4. Wang Q, Yan BH, Jin Y, Cheng Y (2009) Dry reforming of methane in a dielectric barrier discharge reactor with Ni/Al$_2$O$_3$ catalyst: interaction of catalyst and plasma. Energy Fuels 23(18):4196–4201
5. Yan BH, Wang Q, Jin Y, Cheng Y (2010) Dry reforming of methane with carbon dioxide using pulsed DC arc plasma at atmospheric pressure. Plasma Chem Plasma Process 30:257–266
6. Ihara T, Ouro T, Ochiai T, Kiboku M, Iriyama Y (1996) Formation of methanol by microwave plasma reduction of CO$_2$ with H$_2$O. Bull Chem Soc Jpn 69(1):241–244
7. Ihara T, Kiboku M, Iriyama Y (1994) Plasma reduction of CO$_2$ with H$_2$O for the formation of organic compounds. Bull Chem Soc Jpn 67:312–314
8. Liu CJ, Xia Q, Zhang YP, Li Y, Zou JJ, Xu GH, Eliasson B, Xue B (2000) Converting of carbon dioxide into more valuable chemicals using catalytic plasmas. ACS Div Fuel Chem Prep 45:694–697
9. Demidiouk V, Moon S, Chae J, Lee D (2003) Application of a plasma-catalytic system for decomposition of volatile organic compounds. J Korean Phys Soc 42:966–970
10. Kim HH, Ogata A, Futamura S (2007) Complete oxidation of volatile organic compounds (VOCs) using plasma-driven catalytic and oxygen plasma. Plasma Environ Sci Technol 1:46–51
11. Jiang L, Zhu R, Mao Y, Chen J, Zhang L (2015) Conversion characteristics and production evaluation of styrene/o-xylene mixtures removed by DBD pretreatment. Int J Environ Res Publ Health 12:1334–1350

	Journal : **Small 11090**	Dispatch : **31-7-2015**	Pages : **40**
	Article No. : **9640**	☐ LE	☐ TYPESET
	MS Code : **PCPP-15-SV-0038**	☑ CP	☑ DISK

Plasma Chem Plasma Process

922 12. Svirachev DM, Tabaliov NA (2005) Plasma treatment of polymer surfaces in different gases. Bulg J
923   Phys 32:22–33
924 13. Slepička P, Kasálková NS, Stránská E, Bačáková L, Švorčík V (2013) Surface characterization of
925   plasma treated polymers for applications as biocompatible carriers. Express Polym Lett 7(6):535–545
926 14. Borcia C, Borcia G, Dumitrascu N (2011) Surface treatment of polymers by plasma and UV radiation.
927   Rom Rep Phys 56(11):224–232
928 15. Siow KS, Britcher L, Kumar S, Griesser HJ (2006) Plasma methods for the generation of chemically
929   reactive surfaces for biomolecule immobilization and cell colonization—a review. Plasma Process
930   Polym 3:392–418
931 16. Ishaq M, Evans M, Ostrikov K (2014) Effect of atmospheric gas plasmas on cancer cell signaling. Int J
932   Cancer 134:1517–1528
933 17. Alshraiedeh NH, Alkawareek MY, Gorman SP, Graham WG, Gilmore BF (2013) Atmospheric
934   pressure, nonthermal plasma inactivation of MS2 bacteriophage: effect of oxygen concentration on
935   virucidal activity. J Appl Microbiol 115:1420–1426
936 18. Yang B, Chen J, Yu Q, Li H, Lin M, Mustapha A, Hong L, Wang Y (2011) Oral bacterial deactivation
937   using a low-temperature atmospheric argon plasma brush. J Dent 39(1):48–56
938 19. Kostov KG, Rocha V, Koga-Ito CY, Matos BM, Algatti MA, Honda RY, Kayama ME, Mota RP
939   (2010) Bacterial sterilization by a dielectric barrier discharge (DBD) in air. Surf Coat Technol
940   204:2954–2959
941 20. Colagar AH, Sohbatzadeh F, Mirzanejhad S, Omran AV (2010) Sterilization of streptococcus pyo-
942   genes by afterglow dielectric barrier discharge using O_2 and CO_2 working gases. Biochem Eng J
943   51(3):189–193
944 21. Lu W, Cao T, Wang Q, Cheng Y (2011) Plasma-assisted synthesis of chlorinated polyvinyl chloride
945   (CPVC) using a gas-solid contacting process. Plasma Process Polym 8:94–99
946 22. Hessel V, Anastasopoulou A, Wang Q, Kolb G, Lang J (2013) Energy, catalyst and reactor consid-
947   erations for (near)-industrial plasma processing and learning for nitrogen-fixation reactions. Catal
948   Today 211:9–28
949 23. Anastasopoulou A, Wang Q, Hessel V, Lang J (2014) Energy considerations for plasma-assisted
950   N-fixation reactions. Processes 2:694–710
951 24. Cao TF, Zhang HB, Yan BH, Cheng Y (2013) High rate deposition of nanocrystalline silicon by
952   thermal plasma enhanced CVD. Rsc Adv 3:20157–20162
953 25. Cao T, Zhang H, Yan B, Lu W, Cheng Y (2014) Optical emission spectroscopy diagnostic and
954   thermodynamic analysis of thermal plasma enhanced nanocrystalline silicon CVD process. RSC Adv
955   4:15131–15137
956 26. Bhaviripudi S, Mile E, Steiner SA, Zare AT, Dresselhaus MS, Belcher AM, Kong J (2007) CVD
957   synthesis of single-walled carbon nanotubes from gold nanoparticle catalysts. J Am Chem Soc
958   129(6):1516–1517
959 27. Tao X, Zhang X, Cheng J, Liu F, Luo J, Luo Z (2006) Morphology-controllable CVD synthesis of
960   carbon nanomaterials on an alkali-element-doped Cu catalyst. Chem Vap Depos 12:353–356
961 28. Moravec P (2011) NiO_x nanoparticle synthesis by chemical vapor deposition from nickel acetylace-
962   tonate. Mater Sci Appl 2:258–264
963 29. Tang KB, Qian YT, Zeng JH, Yang XG (2003) Solvothermal route to semiconductor nanowires. Adv
964   Mater 15(5):448–450
965 30. Yang J, Zeng JH, Yu SH, Yang L, Zhou GE, Qian YT (2000) Formation process of CdS nanorods via
966   solvothermal route. Chem Mater 12(15):3259–3263
967 31. Chauhan H, Singh MK, Hashmi SA, Deka S (2015) Synthesis of surfactant-free SnS nanorods by a
968   solvothermal route with better electrochemical properties towards supercapacitor applications. RSC
969   Adv. 5:17228–17235
970 32. Rahman IA, Padavettan V (2012) Synthesis of silica nanoparticles by Sol-Gel: size-dependent pro-
971   erties, surface modification, and applications in silica-polymer nanocompositesa review. J Nanomater
972   2012:1–15
973 33. Reda SM (2010) Synthesis of ZnO and Fe_2O_3 nanoparticles by sol-gel method and their application in
974   dye-sensitized solar cells. Mater Sci Semicond Process 13:417–425
975 34. Aparna Y, Venkateswara Rao K, Srinivasa Subbarao P (2012) Preparation and characterization of CuO
976   Nanoparticles by novel sol-gel technique. J Nano-Electron Phys 4(3):4–7
977 35. Ullmann M, Friedlander S, Schmidt-Ott A (2002) Nanoparticle formation by laser ablation. J Nanopart
978   Res 4:499–509
979 36. Amans D, Malaterre C, Diouf M, Mancini C, Chaput F, Ledoux G, Breton G, Guillin Y, Dujardin C,
980   Masenelli-Varlot K, Perriat P (2011) Synthesis of oxide nanoparticles by pulsed laser ablation in

981   liquids containing a complexing molecule: impact on size distributions and prepared phases. J Phys
982   Chem C 115:5131–5139
983 37. Hahn A (2008) Influences on nanoparticle production during pulsed laser ablation. J Laser Micro/
984   Nanoeng 3(2):73–77
985 38. Shimada M, Wang WN, Okuyama K (2010) Synthesis of gallium nitride nanoparticles by microwave
986   plasma-enhanced CVD. Chem Vap Depos 16:151–156
987 39. Ostrikov K (2005) Reactive plasmas as a versatile nanofabrication tool. Rev Mod Phys 77:489–511
988 40. Grasso S, Poetschke J, Richter V, Maizza G, Sakka Y, Reece MJ (2013) Low-temperature spark
989   plasma sintering of pure nano WC powder. J Am Ceram Soc 96:1702–1705
990 41. Tong L, Reddy RG (2005) Synthesis of titanium carbide nano-powders by thermal plasma. Scr Mater
991   52:1253–1258
992 42. Yang YF, Wang HY, Zhao RY, Liang YH, Jiang QC (2008) Effect of Ni content on the reaction
993   behaviors of self-propagating high-temperature synthesis in the Ni–Ti–B$_4$C system. Int J Refract Met
994   Hard Mater 26:77–83
995 43. Rizk S, Assouar MB, Belmahi M, Le Brizoual L, Bougdira J (2007) Synthesis of SiC nanofibers by
996   microwave plasma assisted chemical vapour deposition in CH$_4$/H$_2$ gas mixture. Phys Status Solidi
997   (a) 204(9):3085–3090
998 44. Leconte Y, Leparoux M, Portier X, Herlin-Boime N (2008) Controlled synthesis of β-SiC
999   nanopowders with variable stoichiometry using inductively coupled plasma. Plasma Chem Plasma
1000   Process 28:233–248
1001 45. Ruiz-Camacho J, Castell R, Castro A, Manrique M (2008) Synthesis of silicon carbide in a nitrogen
1002   plasma torch: rotational temperature determination and material analysis. J Phys D Appl Phys
1003   41:175208
1004 46. Kakati M, Bora B, Sarma S, Saikia BJ, Shripathi T, Deshpande U, Dubey A, Ghosh G, Das AK (2008)
1005   Synthesis of titanium oxide and titanium nitride nano-particles with narrow size distribution by
1006   supersonic thermal plasma expansion. Vacuum 82:833–841
1007 47. Tavares J, Coulombe S, Meunier J-L (2009) Synthesis of cubic-structured monocrystalline titanium
1008   nitride nanoparticles by means of a dual plasma process. J Phys D Appl Phys 42:102001
1009 48. Khobta I, Petukhov O, Vasylkiv O, Sakka Y, Ragulya A (2011) Synthesis and consolidation of TiN/
1010   TiB$_2$ ceramic composites via reactive spark plasma sintering. J Alloys Compd 509(5):1601–1606
1011 49. Bora B, Aomoa N, Kakati M, Bhuyan H (2013) Studies on a supersonic thermal plasma expansion
1012   process for synthesis of titanium nitride nanoparticles. Powder Technol 246:413–418
1013 50. Kim K (2005) Plasma synthesis and characterization of nanocrystalline aluminum nitride particles by
1014   aluminum plasma jet discharge. J Cryst Growth 283:540–546
1015 51. Kulkarni NV, Karmakar S, Banerjee I, Sahasrabudhe SN, Das AK, Bhoraskar SV (2009) Growth of
1016   nano-particles of Al$_2$O$_3$, AlN and iron oxide with different crystalline phases in a thermal plasma
1017   reactor. Mater Res Bull 44:581–588
1018 52. Rutkowski PJ, Kata D (2013) Thermal properties of AlN polycrystals obtained by pulse plasma
1019   sintering method. J Adv Ceram 2(2):180–184
1020 53. Kim DW, Kim TH, Park HW, Park DW (2011) Synthesis of nanocrystalline magnesium nitride
1021   (Mg$_3$N$_2$) powder using thermal plasma. Appl Surf Sci 257(12):5375–5379
1022 54. Hou WC, Chen LY, Hong FCN (2008) Fabrication of gallium nitride nanowires by nitrogen plasma.
1023   Diam Relat Mater 17:1780–1784
1024 55. Lee CM, Choi SI, Choi SS, Hong SH (2006) Synthesis of boron nitride nanotubes by arc-jet plasma.
1025   Curr Appl Phys 6:166–170
1026 56. Oh SM, Park DW (2000) Preparation of ultra-fine alumina powders by D. C. plasma jet. Korean J
1027   Chem Eng 17(3):299–303
1028 57. Kumar S, Kang K, Bae G, Selvarajan V, Lee C (2008) Synthesis and characterization of alumina nano-
1029   powders by oxidation of molten aluminium in a thermal plasma reactor: comparison with theoretical
1030   estimation. Mater Chem Phys 11:436–441
1031 58. Im JH, Lee JH, Park DW (2008) Synthesis of nano-sized tin oxide powder by argon plasma jet at
1032   atmospheric pressure. Surf Coat Technol 202:5471–5475
1033 59. Kim JH, Hong YC, Uhm HS (2007) Synthesis of oxide nanoparticles via microwave plasma
1034   decomposition of initial materials. Surf Coat Technol 201:5114–5120
1035 60. Hattori Y, Mukasa S, Toyota H, Inoue T, Nomura S (2011) Synthesis of zinc and zinc oxide
1036   nanoparticles from zinc electrode using plasma in liquid. Mater Lett 65(2):188–190
1037 61. Banerjee I, Karmakar S, Kulkarni NV, Nawale AB, Mathe VL, Das AK, Bhoraskar SV (2010) Effect
1038   of ambient pressure on the crystalline phase of nano TiO$_2$ particles synthesized by a dc thermal plasma
1039   reactor. J Nanopart Res 12:581–590

Journal : **Small 11090**	Dispatch : **31-7-2015**	Pages : **40**
Article No. : **9640**	☐ LE	☐ TYPESET
MS Code : **PCPP-15-SV-0038**	☑ CP	☑ DISK

Plasma Chem Plasma Process

62. Chakravarty U, Naik PA, Mukherjee C, Kumbhare SR, Gupta PD (2010) Formation of metal nanoparticles of various sizes in plasma plumes produced by Ti:sapphire laser pulses. J Appl Phys 108:053107

63. Noguez C (2007) Surface plasmons on metal nanoparticles: the influence of shape and physical environment. J Phys Chem C 111:3806–3819

64. Tavares J, Swanson EJ, Coulombe S (2008) Plasma synthesis of coated metal nanoparticles with surface properties tailored for dispersion. Plasma Process Polym 5:759–769

65. Tailleur A, Achour A, Djouadi MA, Le Brizoual L, Gautron E, Tristant P (2012) PECVD low temperature synthesis of carbon nanotubes coated with aluminum nitride. Surf Coatings Technol 211:18–23

66. Hahn J, Han JH, Yoo JE, Jung HY, Suh JS (2004) New continuous gas-phase synthesis of high purity carbon nanotubes by a thermal plasma jet. Carbon 42:877–883

67. Matsuura T, Taniguchi K, Watanabe T (2007) A new type of arc plasma reactor with 12-phase alternating current discharge for synthesis of carbon nanotubes. Thin Solid Films 515:4240–4246

68. Bystrzejewski M, Huczko A, Lange H, Płotczyk WW, Stankiewicz R, Pichler T, Gemming T, Rümmeli MH (2008) A continuous synthesis of carbon nanotubes by dc thermal plasma jet. Appl Phys A 91:223–228

69. Okada T, Kaneko T, Hatakeyama R (2007) Conversion of toluene into carbon nanotubes using arc discharge plasmas in solution. Thin Solid Films 515:4262–4265

70. Lu FK, Roseberry CM, Meyers JM, Wilson DR, Lee YM, Czysz PA (2004) Pyrolysis of methane in a supersonic, arc-heated flow. Reactions 1–7

71. Fabry F, Flamant G, Fulcheri L (2001) Carbon black processing by thermal plasma. Analysis of the particle formation mechanism. Chem Eng Sci 56(6):2123–2132

72. Baldissarelli VZ, Cassini FA, De Souza IG, Debacher NA (2014) Plasma-assisted production of carbon black and carbon nanotubes from methane by thermal plasma reform. J Braz Chem Soc 25(1):126–132

73. Moreno-Couranjou M, Monthioux M, Gonzalez-Aguilar J, Fulcheri L (2009) A non-thermal plasma process for the gas phase synthesis of carbon nanoparticles. Carbon 47(10):2310–2321

74. Bakken JA, Jensen R, Monsen B, Raaness O, Waernes AN (1998) Thermal plasma process development in Norway. Pure Appl Chem 70(6):1223–1228

75. Naess SN, Elgsaeter A, Helgesen G, Knudsen KD (2009) Carbon nanocones: wall structure and morphology. Sci Technol Adv Mater 10(6):065002

76. Fulcheri L, Schwob Y, Fabry F, Flamant G, Chibante LFP, Laplaze D (2000) Fullerene production in a 3-phase AC plasma process. Carbon 38(6):797–803

77. Weidong X, Fulcheri L, Gonzalez-Aguilar J, Hui L, Gruenberger TM (2006) Characterization of a 3-Phase a.c. Free burning arc plasma. Plasma Sci Technol 8(2):156–163

78. Gonzalez-Aguilar J, Moreno M, Fulcheri L (2007) Carbon nanostructures production by gas-phase plasma processes at atmospheric pressure. J Phys D Appl Phys 40(8):2361–2374

79. Mariotti D, Ostrikov K (2009) Tailoring microplasma nanofabrication: from nanostructures to nanoarchitectures. J Phys D Appl Phys 42:092002

80. Mariotti D, Sankaran RM (2010) Microplasmas for nanomaterials synthesis. J Phys D Appl Phys 43:323001

81. Belmonte T, Arnoult G, Henrion G, Gries T (2011) Nanoscience with non-equilibrium plasmas at atmospheric pressure. J Phys D Appl Phys 44:363001

82. Mariotti D (2008) Nonequilibrium and effect of gas mixtures in an atmospheric microplasma. Appl Phys Lett 92:3–5

83. Kurunczi P, Shah H, Becker K (1999) Hydrogen Lyman-α and Lyman-β emissions from high-pressure microhollow cathode discharges in Ne–H_2 mixtures. J Phys B: At Mol Opt Phys 32:L651–L658

84. Kurunczi P, Lopez J, Shah H, Becker K (2001) Excimer formation in high-pressure microhollow cathode discharge plasmas in helium initiated by low-energy electron collisions. Int J Mass Spectrom 205:277–283

85. Belostotskiy SG, Khandelwal R, Wang Q, Donnelly VM, Economou DJ, Sadeghi N (2008) Measurement of electron temperature and density in an argon microdischarge by laser Thomson scattering. Appl Phys Lett 92:1–4

86. Rajesh R, Kumar BR, Varshney SK, Kumar M, Chavda C, Thakkar A, Patel NC, Kumar A, Team A (2000) Electron temperature measurements by Thomson scattering system. Pramana 55:733–740

87. Frank K, Ernst U, Petzenhauser WH (2001) Proceedings of Record IEEE international conference on the plasma science. Las Vegas, NV, p 381

1098 88. El-Habachi A, Moselhy M, Stark RH, Schoenbach KH (2000) Excimer emission from microhollow
1099   cathode discharges. ICOPS 2000 IEEE conference Rec-Abstr 27th IEEE international conference on
1100   plasma science (Cat No.00CH37087). doi:10.1109/PLASMA.2000.855103
1101 89. Moselhy M, Shi W, Stark RH, Schoenbach KH (2001) Xenon excimer emission from pulsed
1102   microhollow cathode discharges. Appl Phys Lett 79:1240–1242
1103 90. Gill P, Webb CE (2001) Electron energy distributions in the negative glow and their relevance to
1104   hollow cathode lasers. J Phys D Appl Phys 10:299–301
1105 91. Iza F, Lee JK, Kong MG (2007) Electron kinetics in radio-frequency atmospheric-pressure
1106   microplasmas. Phys Rev Lett 99:2–5
1107 92. Choi J, Iza F, Lee JK, Ryu CM (2007) Electron and ion kinetics in a DC microplasma at atmospheric
1108   pressure. IEEE Trans Plasma Sci 35(5):1274–1278
1109 93. Zhu XM, Walsh JL, Chen WC, Pu YK (2012) Measurement of the temporal evolution of electron
1110   density in a nanosecond pulsed argon microplasma: using both Stark broadening and an OES line-ratio
1111   method. J Phys D Appl Phys 45:295201
1112 94. Zhu XM, Chen WC, Pu YK (2008) Gas temperature, electron density and electron temperature
1113   measurement in a microwave excited microplasma. J Phys D Appl Phys 41:105212
1114 95. Iza F, Hopwood JA (2005) Self-organized filaments, striations and other nonuniformities in non-
1115   thermal atmospheric microwave excited microdischarges. IEEE Trans Plasma Sci 33(2):306–307
1116 96. McKay K, Iza F, Kong MG (2010) Excitation frequency effects on atmospheric-pressure helium RF
1117   microplasmas: plasma density, electron energy and plasma impedance. Eur Phys J D 60:497–503
1118 97. Souza-Corrêa JA, Oliveira C, Gomes MP, Amorim J (2010) Electric and spectroscopic properties of
1119   argon-hydrogen RF microplasma jets at atmospheric pressure. J Phys D Appl Phys 43:395203
1120 98. Tachibana K (2006) Current status of microplasma research. IEEJ Trans Electr Electron Eng
1121   1:145–155
1122 99. Shimada M, Tynan GR, Cattolica R (2006) Rotational and translational temperature equilibrium in an
1123   inductively coupled plasma. J Vac Sci Technol, A 24(5):1878–1883
1124 100. Bazavan M, Iova I (2008) Temperature determination of a cold N2 discharge plasma by the fit of the
1125   experimental spectra with the simulated emission spectra. Rom Rep Phys 60(3):671–678
1126 101. Foest R, Schmidt M, Becker K (2006) Microplasmas, an emerging field of low-temperature plasma
1127   science and technology. Int J Mass Spectrom 248:87–102
1128 102. Block R, Toedter O, Schoenbach KH (1999) Proceedings of the 30th AIAA plasma dynamics and
1129   lasers conference. Norfolk. Paper no. AIAA-99-3434
1130 103. Block R, Laroussi M, Leipold F, Schoenbach KH (1999) Proceedings of the 14th international
1131   symposium on plasma chemistry. Prague, Czech Republic, p 945
1132 104. Lin PA (2012) Design and fabrication of compositionally and shape controlled metal nanoparticles for
1133   semiconductor nanowire growth. Case Western Reserve University, New York
1134 105. Penache C, Miclea M, Demian AB, Hohn O, Schossler S, Jahnke T, Niemax K, Bocking HS (2002)
1135   Characterization of a high-pressure microdischarge using diode laser atomic absorption spectroscopy.
1136   Plasma Sources Sci Technol 11:476–483
1137 106. Becker K, Koutsospyros A, Yin SM, Christodoulatos C, Abramzon N, Joaquin JC, Marino GB (2005)
1138   Environmental and biological applications of microplasmas. Plasma Phys Control Fusion 47:B513–
1139   B523
1140 107. Seto T, Kwon SB, Hirasawa M, Yabe A (2005) Decomposition of toluene with surface-discharge
1141   microplasma device. Jpn J Appl Phys 44:5206–5210
1142 108. Mohamed AAH, Block R, Schoenbach KH (2002) Direct current glow discharges in atmospheric air.
1143   IEEE Trans Plasma Sci 30(1):182–183
1144 109. Mizeraczyk J, Hrycak B, Jasinski M (2012) Low-temperature microwave microplasma for bio-de-
1145   contamination. Przegląd Elektrotechniczny 88(9):238–241
1146 110. Kurunczi P, Martus KE, Becker K (2013) Neon excimer emission from pulsed high-pressure micro-
1147   hollow cathode discharge plasmas. Int J Mass Spectrom 223–224:37–43
1148 111. Masoud N, Martus K, Becker K (2004) Vacuum ultraviolet emissions from a cylindrical dielectric
1149   barrier discharge in neon and neon-hydrogen mixtures. Int J Mass Spectrom 233:395–403
1150 112. Moselhy M, Stark RH, Schoenbach KH, Kogelschatz U (2001) Resonant energy transfer from argon
1151   dimers to atomic oxygen in microhollow cathode discharges. Appl Phys Lett 78:880–882
1152 113. El-Habachi A, Schoenbach KH (1998) Generation of intense excimer radiation from high-pressure
1153   hollow cathode discharges. Appl Phys Lett 73:885–887
1154 114. El-Habachi A, Shi W, Moselhy M, Stark RH, Schoenbach KH (2000) Series operation of direct current
1155   xenon chloride excimer sources. J Appl Phys 88(6):3220–3224
1156 115. Sladek REJ, Stoffels E, Walraven R, Tielbeek PJA, Koolhoven RA (2004) Plasma treatment of dental
1157   cavities: a feasibility study. IEEE Trans Plasma Sci 32(4):2002–2005

116. Shimizu K, Fukunaga H, Tatematsu S, Blajan M (2012) Atmospheric microplasma application for surface modification of biomaterials. Jpn J Appl Phys 51:11PJ01

117. Blajan M, Umeda A, Shimizu K (2013) Surface treatment of glass by microplasma. IEEE Trans Ind Appl 49(2):714–720

118. Eden JG, Park SJ, Ostrom NP, Chen KF (2005) Recent advances in microcavity plasma devices and arrays: a versatile photonic platform. J Phys D Appl Phys 38:1644–1648

119. Ichiki T, Koidesawa T, Horiike Y (2003) An atmospheric-pressure microplasma jet source for the optical emission spectroscopic analysis of liquid sample. Plasma Sources Sci Technol 12:S16–S20

120. Shimizu K, Fukunaga H, Blajan M (2014) Biomedical applications of atmospheric microplasma. Curr Appl Phys 14:S154–S161

121. Chiang WH, Sakr M, Gao XPA, Sankaran RM (2009) Nanoengineering Ni_xFe_{1-x} catalysts for gas-phase, selective synthesis of semiconducting single-walled carbon nanotubes. ACS Nano 3(12):4023–4032

122. Martin V, Bauville G, Sadeghi N, Puech V (2011) Microplasmas as vacuum ultraviolet source for Cl-atom density measurements by resonance absorption spectroscopy. J Phys D Appl Phys 44:435203

123. Park JB, Oh JS, Gil E, Kyoung SJ, Kim JS, Yeom GY (2009) Plasma texturing of multicrystalline silicon for solar cell using remote-type pin-to-plate dielectric barrier discharge. J Phys D Appl Phys 42:215201

124. Chiang WH, Richmonds C, Sankaran RM (2010) Continuous-flow, atmospheric-pressure microplasmas: a versatile source for metal nanoparticle synthesis in the gas or liquid phase. Plasma Sources Sci Technol 19:034011

125. Becker KH, Schoenbach KH, Eden JG (2006) Microplasmas and applications. J Phys D Appl Phys 39:R55–R70

126. Shimizu Y, Sasaki T, Chandra Bose A, Terashima K, Koshizaki N (2006) Development of wire spraying for direct micro-patterning via an atmospheric-pressure UHF inductively coupled microplasma jet. Surf Coat Technol 200:4251–4256

127. Singh PK, Hopwood J, Sonkusale S (2014) Metamaterials for remote generation of spatially controllable two dimensional array of microplasma. Sci Rep 4:5964

128. Chiang WH, Sankaran RM (2008) Synergistic effects in bimetallic nanoparticles for low temperature carbon nanotube growth. Adv Mater 20:4857–4861

129. Lin PA, Sankaran RM (2011) Plasma-assisted dissociation of organometallic vapors for continuous, gas-phase preparation of multimetallic nanoparticles. Angew Chem Int Ed 50:10953–10956

130. Kumar A, Ann Lin P, Xue A, Hao B, Khin Yap Y, Sankaran RM (2013) Formation of nanodiamonds at near-ambient conditions via microplasma dissociation of ethanol vapour. Nat Commun 4:2618

131. Shimizu Y, Bose AC, Mariotti D, Sasaki T, Kirihara K, Suzuki T, Terashima K, Koshizaki N (2006) Reactive evaporation of metal wire and microdeposition of metal oxide using atmospheric pressure reactive microplasma jet. Jpn J Appl Phys 45:8228–8234

132. Bose AC, Shimizu Y, Mariotti D, Sasaki T, Terashima K, Koshizaki N (2006) Flow rate effect on the structure and morphology of molybdenum oxide nanoparticles deposited by atmospheric-pressure microplasma processing. Nanotechnology 17:5976–5982

133. Mariotti D, Svrcek V, Kim DG (2007) Self-organized nanostructures on atmospheric microplasma exposed surfaces. Appl Phys Lett 91:2005–2008

134. Mariotti D, Lindstrom H, Bose AC, Ostrikov K (2008) Monoclinic β-MnO_3 nanosheets produced by atmospheric microplasma: application to lithium-ion batteries. Nanotechnology 19:495302

135. Shimizu Y, Kawaguchi K, Sasaki T, Koshizaki N (2009) Generation of room-temperature atmospheric H_2/Ar microplasma jet driven with pulse-modulated ultrahigh frequency and its application to gold nanoparticle preparation. Appl Phys Lett 94:2007–2010

136. Mariotti D, Bose AC, Ostrikov K (2009) Atmospheric-microplasma-assisted nanofabrication: metal and metal-oxide nanostructures and nanoarchitectures. IEEE Trans Plasma Sci 37(6):1027–1033

137. Kona S, Kim JH, Harnett CK, Sunkara MK (2009) Carbon nanotube growth studies using an atmospheric, microplasma reactor. IEEE Trans Nanotechnol 8(3):286–290

138. Shirai H, Kobayashi T, Hasegawa Y (2005) Synthesis of silicon nanocones using rf microplasma at atmospheric pressure. Appl Phys Lett 87:143112

139. Nozaki T, Sasaki K, Ogino T, Asahi D, Okazaki K (2007) Microplasma synthesis of tunable photoluminescent silicon nanocrystals. Nanotechnology 18:235603

140. Suzuki T, Kato M, Shimizu Y (2013) Fabrication of titanium-based hard coatings by atmospheric microplasma-metal organic chemical vapor deposition using titanium tetraisopropoxide. Int J Autom Technol 7(6):720–725

141. Yoshiki H, Mitsui T (2008) TiO_2 thin film coating on a capillary inner surface using atmospheric-pressure microplasma. Surf Coat Technol 202:5266–5270

	Journal : **Small 11090**	Dispatch : **31-7-2015**	Pages : **40**
	Article No. : **9640**	☐ LE	☐ TYPESET
	MS Code : **PCPP-15-SV-0038**	☑ CP	☑ DISK

Plasma Chem Plasma Process

1218 142. Koh TL, O'Hara EC, Gordon MJ (2012) Microplasma-based synthesis of vertically aligned metal
1219   oxide nanostructures. Nanotechnology 23:425603
1220 143. Yang Z, Shirai H, Kobayashi T, Hasegawa Y (2007) Synthesis of Si nanocones using rf microplasma
1221   at atmospheric pressure. Thin Solid Films 515:4153–4158
1222 144. Shimizu Y, Sasaki T, Ito T, Terashima K, Koshizaki N (2003) Fabrication of spherical carbon via UHF
1223   inductively coupled microplasma CVD. J Phys D Appl Phys 36:2940–2944
1224 145. Cao Z, Walsh JL, Kong MG (2009) Atmospheric plasma jet array in parallel electric and gas flow
1225   fields for three-dimensional surface treatment. Appl Phys Lett 94:021501
1226 146. Li CJ, Sun B (2004) Microstructure and property of Al_2O_3 coating microplasma-sprayed using a novel
1227   hollow cathode torch. Mater Lett 58:179–183
1228 147. Akolkar R, Sankaran RM (2013) Charge transfer processes at the interface between plasmas and
1229   liquids. J Vac Sci Technol, A 31:050811
1230 148. Ghosh S, Bishop B, Morrison I, Akolkar R, Scherson D, Mohan Sankaran R (2015) Generation of a
1231   direct-current, atmospheric-pressure microplasma at the surface of a liquid water microjet for con-
1232   tinuous plasma-liquid processing. J Vac Sci Technol, A 33:021312
1233 149. Lu Y, Xu SF, Zhong XX, Ostrikov K, Cvelbar U, Mariotti D (2013) Characterization of a DC-driven
1234   microplasma between a capillary tube and water surface. Europhys Lett 102:15002
1235 150. Huang XZ, Zhong XX, Lu Y, Li YS, Rider AE, Furman SA, Ostrikov K (2013) Plasmonic Ag
1236   nanoparticles via environment-benign atmospheric microplasma electrochemistry. Nanotechnology
1237   24:095604
1238 151. Huang X, Li Y, Zhong X (2014) Effect of experimental conditions on size control of Au nanoparticles
1239   synthesized by atmospheric microplasma electrochemistry. Nanoscale Res Lett 9(1):572
1240 152. Wang R, Zuo S, Zhu W, Zhang J, Fang J (2014) Rapid synthesis of aqueous-phase magnetite
1241   nanoparticles by atmospheric pressure non-thermal microplasma and their application in magnetic
1242   resonance imaging". Plasma Process Polym 11:448–454
1243 153. Du C, Xiao M (2014) Cu_2O nanoparticles synthesis by microplasma. Sci Rep 4:7339
1244 154. Hieda J, Saito N, Takai O (2008) Exotic shapes of gold nanoparticles synthesized using plasma in
1245   aqueous solution. J Vac Sci Technol, A 26(4):854–856
1246 155. Imasaka K, Kato Y, Suehiro J (2007) Enhancement of microplasma-based water-solubilization of
1247   single-walled carbon nanotubes using gas bubbling in water. Nanotechnology 18:335602
1248 156. Hadzifejzovic E, Elahi A, Caruana DJ (2012) Control of oxidation state of copper in flame deposited
1249   films. Thin Solid Films 520(16):5254–5259
1250 157. Cserfalvi T, Mezei P (1994) Direct solution analysis by glow discharge: electrolyte-cathode discharge
1251   spectrometry. J Anal At Spectrom 9:345–349
1252 158. Lukes P, Appleton AT, Locke BR (2004) Hydrogen peroxide and ozone formation in hybrid gas-liquid
1253   electrical discharge reactors. IEEE Trans Ind Appl 40(1):60–67
1254 159. Shahbazali E, Hessel V, Noël T, Wang Q (2014) Metallic nanoparticles made in flow and their
1255   catalytic applications in organic synthesis. Nanotechnol Rev 3:65–86
1256 160. Kulbe N, Höfft O, Ulbrich A, Zein El Abedin S, Krischok S, Janek J, Pölleth M, Endres F (2011)
1257   Plasma electrochemistry in 1-butyl-3-methylimidazolium dicyanamide: copper nanoparticles from
1258   CuCl and $CuCl_2$. Plasma Process Polym 8:32–37
1259 161. Toriyabe Y, Watanabe S, Yatsu S, Shibayama T, Mizuno T (2007) Controlled formation of metallic
1260   nanoballs during plasma electrolysis. Appl Phys Lett 91:041501
1261 162. Tomai T, Katahira K, Kubo H, Shimizu Y, Sasaki T, Koshizaki N, Terashima K (2007) Carbon
1262   materials syntheses using dielectric barrier discharge microplasma in supercritical carbon dioxide
1263   environments. J Supercrit Fluids 41:404–411
1264 163. Sperling RA, Gil PR, Zhang F, Zanella M, Parak WJ (2008) Biological applications of gold
1265   nanoparticles. Chem Soc Rev 37:1896–1908
1266 **AQ4** 164. Conde J, Doria G, Baptista P (2012) Noble metal nanoparticles applications in cancer. J Drug Deliv 751075
1267 165. Doria G, Conde J, Veigas B, Giestas L, Almeida C, Assunção M, Rosa J, Baptista PV (2012) Noble
1268   metal nanoparticles for biosensing applications. Sensors 12:1657–1687
1269 166. Chiang WH, Sankaran RM (2007) Microplasma synthesis of metal nanoparticles for gas-phase studies
1270   of catalyzed carbon nanotube growth. Appl Phys Lett 91:121503
1271 167. Chiang WH (2009) Engineering nanocatalysts for selective growth of carbon nanotubes. Case Western
1272   Reserve University, USA
1273 168. Askari S, Levchenko I, Ostrikov K, Maguire P, Mariotti D (2014) Crystalline Si nanoparticles below
1274   crystallization threshold: effects of collisional heating in non-thermal atmospheric-pressure
1275   microplasmas. Appl Phys Lett 104:163103
1276 169. Du B, Mohr S, Luggenhölscher D, Czarnetzki U (2011) An atmospheric pressure self-pulsing micro
1277   thin-cathode discharge. J Phys D Appl Phys 44:125204

170. Sankaran RM, Holunga D, Flagan RC, Giapis KP (2005) Synthesis of blue luminescent Si nanoparticles using atmospheric-pressure microdischarges. Nano Lett 5(3):537–541

171. Mangolini L, Thimsen E, Kortshagen U (2005) High-yield plasma synthesis of luminescent silicon nanocrystals. Nano Lett 5(4):655–659

172. Barwe B, Stein A, Cibulka OE, Pelant I, Ghanbaja J, Belmonte T, Benedikt J (2014) Generation of silicon nanostructures by atmospheric microplasma jet: the role of hydrogen admixture. Plasma Process Polym 12(2):132–140

173. Peng KQ, Wang X, Li L, Hu Y, Lee ST (2013) Silicon nanowires for advanced energy conversion and storage. Nano Today 8:75–97

174. Schmidt V, Wittemann JV, Senz S, Gósele U (2009) Silicon nanowires: a review on aspects of their growth and their electrical properties. Adv Mater 21:2681–2702

175. Hasan M, Huq MF, Mahmood ZH (2013) A review on electronic and optical properties of silicon nanowire and its different growth techniques. Springerplus 2(1):151

176. Garnett E, Yang P (2010) Light trapping in silicon nanowire solar cells. Nano Lett 10(3):1082–1087

177. Bogart TD, Oka D, Lu X, Gu M, Wang C, Korgel BA (2014) Lithium ion battery performance of silicon nanowires with carbon skin. ACS Nano 8(1):915–922

178. Chen KI, Li BR, Chen YT (2011) Silicon nanowire field-effect transistor-based biosensors for biomedical diagnosis and cellular recording investigation. Nano Today 6(2):131–154

179. Barborini E, Ducati C, Leccardi M, Bertolini G, Repetto P, Milani P (2011) Nanostructured refractory metal oxide films produced by a pulsed microplasma cluster source as active layers in microfabricated gas sensors. Jpn J Appl Phys 50:01AK01

180. Li Y, Della Valle F, Simonnet M, Yamada I, Delaunay JJ (2009) High-performance UV detector made of ultra-long ZnO bridging nanowires. Nanotechnology 20:045501

181. Liu G, Gao J, Ai H, Chen X (2013) Applications and potential toxicity of magnetic iron oxide nanoparticles. Small 9(9):1533–1545

182. Iida C, Sato M, Nakayama M, Sanada A (2011) Electrodeposition of Cu_2O nanopyramids using an anodic aluminum oxide template. Int J Electrochem Sci 6:4730–4736

183. Tiwari DK, Behari J, Sen P (2008) Application of nanoparticles in waste water treatment. Carbon Nanotube 3(3):417–433

184. Hashimoto K, Irie H, Fujishima A (2005) TiO_2 photocatalysis: a historical overview and future prospects. Jpn J Appl Phys 44(12):8269–8285

185. Ruppi S (2005) Deposition, microstructure and properties of texture-controlled CVD α-Al_2O_3 coatings. Int J Refract Met Hard Mater 23:306–316

186. Eskandari A, Sangpour P, Vaezi MR (2014) Hydrophilic Cu_2O nanostructured thin films prepared by facile spin coating method: investigation of surface energy and roughness. Mater Chem Phys 147(3):1204–1209

187. Lee YJ, Seo YI, Kim SH, Kim DG, Kim YD (2009) Deposition of Mo oxide and metallic Mo films by chemical vapor transport of $MoO_3(OH)_2$. Chem Vap Depos 15:199–203

188. Yoshiki H, Orada T, Hirai K, Hatakeyama R (2006) Growth of vertically aligned carbon nanotube bundles using atmospheric-pressure microplasma. Jpn J Appl Phys 45:9276–9279

189. Sankaran RM, Giapis KP (2002) Hollow cathode sustained plasma microjets: characterization and application to diamond deposition. J Appl Phys 92:2406–2411

190. Zou Q, Wang MZ, Li YG, Zhou LH (2009) Fabrication of carbon nanomaterials using pulse microplasma in SEM. Plasma Dev Oper 17:175–180

191. Levchenko I, Ostrikov K, Mariotti D, Švrček V (2009) Self-organized carbon connections between catalyst particles on a silicon surface exposed to atmospheric-pressure Ar + CH_4 microplasmas. Carbon 47:2379–2390

192. Mochalin VN, Shenderova O, Ho D, Gogotsi Y (2011) The properties and applications of nanodiamonds. Nat Nanotechnol 7(1):11–23

193. Zhang Q, Mochalin VN, Neitzel I, Knoke IY, Han J, Klug CA, Zhou JG, Lelkes PI, Gogotsi Y (2011) Fluorescent PLLA-nanodiamond composites for bone tissue engineering. Biomaterials 32(1):87–94

194. De Volder MFL, Tawfick SH, Baughman RH, Hart AJ (2013) Carbon nanotubes: present and future commercial applications. Science 339:535–539

195. Shin SR, Bae H, Cha JM, Mun JY, Chen YC, Tekin H, Shin H, Farshchi S, Dokmeci MR, Tang S, Khademhosseini A (2012) Carbon nanotube reinforced hybrid microgels as scaffold materials for cell encapsulation. ACS Nano 6(1):362–372

196. Kordás K, Tóth G, Moilanen P, Kumpumäki M, Vähäkangas J, Uusimäki A, Vajtai R, Ajayan PM (2007) Chip cooling with integrated carbon nanotube microfin architectures. Appl Phys Lett 90:5–7

197. Yang Z, Kikuchi T, Hatou Y, Kobayashi T, Shirai H (2005) Carbon microstructures synthesized utilizing the RF microplasma jet at atmospheric pressure. Jpn J Appl Phys 44:4122–4127

Springer

the language of science

Author Query Form

Please ensure you fill out your response to the queries raised below and return this form along with your corrections

Dear Author

During the process of typesetting your article, the following queries have arisen. Please check your typeset proof carefully against the queries listed below and mark the necessary changes either directly on the proof/online grid or in the 'Author's response' area provided below

Query	Details Required	Author's Response
AQ1	Please check and confirm the edit made in figure legends and the part labels inserted in figures.	
AQ2	The labels in Fig. 11 is not readable. Please provide a new figure with legible labels in Vector EPS or tiff/jpeg format with 600 dpi resolution.	
AQ3	Please update Ref. [70] with volume number.	
AQ4	Please update Ref. [164] with volume and page numbers.	